UNIVERSITÀ DEGLI STUDI DI PALERMO

Dottorato di Ricerca in Oncologia e Chirurgia Sperimentali
Dipartimento di Discipline Chirurgiche, Oncologiche e Stomatologiche (Di.Chir.On.S.)
Settori Scientifici Disciplinari MED/28 e CHIM/09

NEW GUIDED BONE REGENERATION PROCEDURE USING LEUKOCYTE- AND PLATELET-RICH FIBRIN (L-PRF) IN ORAL SURGERY

DOCTORAL DISSERTATION OF:
DENISE MURGIA

THE CHAIR OF THE DOCTORAL PROGRAM:
PROF. ANTONIO RUSSO

TUTOR
PROF. GIUSEPPINA CAMPISI

CO TUTOR
PROF. VIVIANA DE CARO

CYCLE XXXIII
ATTAINMENT YEAR 2021

UNIVERSITÀ DEGLI STUDI DI PALERMO

INDEX

UNIVERSITÀ DEGLI STUDI DI PALERMO

ABSTRACT

Non-transfusional hemocomponents are autogenous products used in several surgical fields obtained by the centrifugation of a blood sample from a patient and able to promote hard and soft tissue regeneration, local haemostasis, and the acceleration of wound healing.

The aim of this PhD thesis was the validation of an innovative protocol for the Guided Bone Regeneration (GBR) technique using second-generation autologous platelet concentrates, Leukocytes and Platelet-rich Fibrin (L-PRF), in post-extraction sockets of patients in need of dental avulsions and successive implant prosthetic rehabilitation, evaluating its ability to prevent alveolar bone resorption and promote bone regeneration.

The secondary aim was the design and development of a multicomposite loaded with antimicrobic and antioxidant agents, to be applied wrapped in the L-PRF membrane, enhancing its regenerative properties.

This project cohering with the National Operational Program (PON) “Research and Innovation” (R&I) 2014-2020 funding by the Italian Ministry of Education, University and Research, aimed to promote the research and the innovation of the country, with a particular interest on the Health Specialization Area.

SUMMARY

Teeth extractions are common practices in oral surgery, but they are often followed by alveolar bone resorption and remodeling processes, that can lead to significant changes in ridge dimensions, both horizontal and vertical. Dental implants are the most common choice to replace tooth extracted, but to achieve the ideal functional and aesthetic prosthetic rehabilitation, the adequate alveolar bone volume is required.

To prevent the development of severe bone resorption and provide the adequate bone height and width for implant restoration, several surgical techniques have been proposed, such as guided bone regeneration procedures (GBR) and alveolar ridge preservation (ARP). The use of resorbable membranes and autologous bone grafts is currently the "gold standard" of the GBR procedures even though they present some drawbacks such as morbidity of the additional surgical site, limited graft accessibility, risk of clinical complication, prolonged operation time and high cost of interventions. The use of non-transfusional hemocomponents in GBR and ARP techniques have been defined as an innovative strategy to achieve soft and hard tissue healing in the post-extraction sockets, overcoming the drawbacks of the traditional procedures. Recently, leukocyte and platelet-rich fibrin (L-PRF) and its derivate PRF-Block has been applied in regenerative procedures, exhibited promising results.

Indeed, the aim of this thesis was the validation of a GBR protocol based on the use of L-PRF on the post-extraction sockets of patients in need of dental extraction and successive implant prosthetic rehabilitation. The ability of these systems to prevent alveolar bone resorption in the alveolus and promote bone regeneration in various-size bony defects have been evaluated to validate the proposed surgical procedure. Five patients were treated by GBR procedures to regenerate three-dimensional bone defects and, in other ten patients, ARPs were performed to prevent alveolar bone resorption. The achievement of the adequate ridge dimensions allowed successful implant-based rehabilitation in all the enrolled subjects. The obtained outcomes in terms of bone healing and tissue regeneration were in accordance with the literature and reinforce the effective role of L-PRF and its derivate in oral surgical procedures.

The secondary aim was the development of a multicomposite biomaterial based on nanostructured lipid carriers loaded with lipophilic antioxidant compound and entrapped in a biodegradable matrix loaded with an antibiotic, to be applied in association with the L-PRF membrane, enhancing its regenerative properties.

CHAPTER 1

Background, Rationale and Objectives

a) Leucocytes and Platelet rich Fibrin (L-PRF) for Guided Bone Regeneration and Alveolar Ridge Preservation

1.1 Mechanisms of Bone Formation and Development

Bone is a connective tissue providing protection for internal organs and tissues, mechanical support for muscles, depot for the systemic mineral homeostasis, such as calcium, phosphate, amino acids, and bicarbonate, and mastication. It also performs metabolic functions, including the secretion of hormones that regulate both mineral and energy metabolism. To accomplish these functions, two types of bone could be recognized, with different morphology and functionality[1].

The cortical component, or compact bone, accounts for almost 80% of skeletal mass, owns mechanical and protective functions and is located in diaphyseal regions of long bones. It is characterized by densely formed collagen fibrils surrounding a central channel for blood vessels, lymphatics, and nerves.

Trabecular bone, also known as cancellous bone, is located inside the cortical one at the ends of long bones, where the compact is thinner. It is a spongy tissue made by a porous network of thin wires, called trabeculae, having metabolic functions and able to transfers mechanical loads from the articular surface to the cortical bone and absorb shock for its hydraulic properties[2].

The surface to volume ratio in cortical bone is much lower than in trabecular, that has less calcium but more water content and a higher turnover[1]. Indeed, bone tissue has a dynamic nature, characterized by the constant formation of new bone and dissolution of old, injured, or unnecessary ones for repair or calcium release and it can constantly adapt to the surrounding environment.

Bone is made up of cells and extracellular matrix and the osteogenesis, the process of bone formation, can be distinguished in endochondral, intramembranous, or sutural[3].

The extracellular matrix is a highly mineralized tissue, produced by osteoblasts. These cells are responsible for the new bone formation, derived from multipotent mesenchymal stem cells

(MSCs) in the bone marrow and placed especially in the growing portions of bone. By contrary, the cells responsible for bone resorption, or breakdown, are the osteoclasts derived from hematopoietic progenitors (i.e., monocytes/macrophages) found also in the bone marrow[4]. The remodeling process of bone exceeds in bone formation during the growth stages of childhood, adolescence and into young adulthood; after this stage, bone resorption outperforms bone formation, leading to a gradual and progressive bone loss[2]. The endocortical surface is exposed to the marrow and the solid bone and often shows a higher bone turnover than other trabecular or cortical surfaces[1].

Bone regeneration is a complex, well-orchestrated physiological process of bone formation, occurring in normal fracture healing, and involved in a continuous remodeling throughout adult life[5]. Bone turnover, and, consequently, bone mass can be influenced by several systemic factors, such as nutrition, hormonal status, exposure to smoking, alcohol, physical inactivity, or particular drugs[3]. Besides, on account of the declining estrogens at menopause, usually, women have a more rapid bone loss and a greater risk of osteoporosis than men[6].

The differentiation of MSCs in osteoblast is stimulated by specific transcription factors since these cells are the progenitors of either adipocytes, chondrocytes, or myoblasts[7,8]. The essential regulators of osteoblast differentiation are runt-related transcription factor 2 (RUNX2) and Osterix downstream of RUNX2 that, during the proliferation phase, stimulate a morphological change from osteoprogenitors to pre-osteoblasts, which start to synthetize bone matrix and alkaline phosphatase (ALP)[9]. Mature osteoblasts then regulate bone matrix mineralization and produce osteocalcin (OCN) that, with ALP, are used as clinical markers of bone formation[9].

Instead, osteoclasts differentiation is promoted by a bond between receptor activator of NF-kB ligand (Tnfsf11/RANKL) secreted by osteoblasts and RANK receptors located on the surface of hematopoietic cells[10]. During osteoclastogenesis, bone marrow macrophages (BMMs) differentiate into tartrate-resistant acid phosphatase (TRAP)-positive pre-osteoclasts, which then fuse to form mature osteoclasts[7,11]. RANKL and macrophage colony-stimulating factor (M-CSF) are two markers of osteoclasts formation[11], while osteoblast-secreted osteoprotegerin (OPG) acts as a decoy receptor inhibiting the interaction between RANKL and RANK[12].

Systemic and local factors, such as bone morphogenetic proteins, canonical wingless (Wnt)/β-catenin signaling pathway, insulin-like growth factor (IGF), mechanical forces, estrogen and other hormones could influence transcription factors activity, thus bone turnover[4,10].

1.2 Alveolar bone

The portion of maxilla and mandible that forms tooth sockets is characterized by a rapid remodeling due to tooth eruption and functional demands; it provides support to the teeth by an attachment apparatus based on three tissues: root cementum, periodontal ligament and alveolar bone[13,14] (Figure 1).

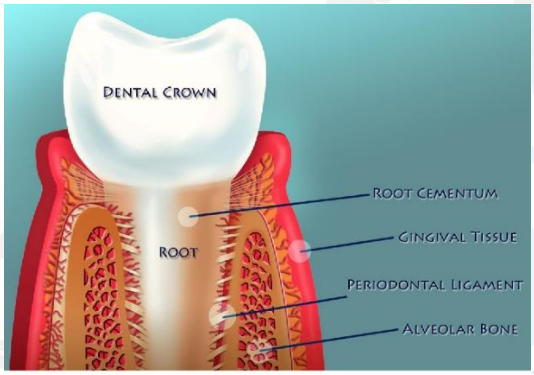

Figure 1 Periodontal tissues: gingiva, periodontal ligament, root cementum, and alveolar bone[15].

The alveolar bone develops into an intramembranous bone formation during the creation of the mandible and maxilla, in concomitance of the primary dentition. During this process, bone develops around the inferior alveolar nerve and the incisive nerve, forming the bony trough within which the nerve will lay, and that will house the developing tooth buds[13]. It is the major support structure for the teeth, provides a framework to the marrow and attachment to the forming periodontal ligament (PDL) and the muscles; it also absorbs the pressures generated during tooth contacts and serves as a reservoir of Calcium and other ions[16].

Two components could be described: the alveolar bone proper and alveolar bone process.

The former provides the attachment site for the PDL, lining the tooth socket[17]. The insertion of Sharpey's fibres into alveolar bone proper is the key to tooth root housing. These fibres are organized in bundles and calcified within the bone to provide a strong attachment between tooth and bone[17]. The latter type houses the developing tooth buds first and once erupted, the roots of the teeth and provides structural support for the dentition; this type is usually affected by tooth loss, resorbing after becoming unnecessary.

The bone process is composed of an outer layer of cortical bone and an inner region of cancellous bone and contains the blood vessels and nerves that support the teeth and the bone marrow with the adipose and osteogenic cells and the hemopoietic tissue.

The portion on alveolar bone process nearest to the Sharpey's fibres is also known as Bundle Bone, due to the presence of the fibre bundles and it plays a key role into tooth movement and disease processes involving the periodontium[18]. Instead, the Lamellar Bone is a section of the alveolar bone proper, perforated by numerous small foramina that allow nerve and vessel irrigation until the PDL tissues. The coronal margin of the bone, lining the socket, becomes the alveolar crest, that results more mineralized than the bone adjacent to the apex of the tooth[13].

Thus, in general, alveolar bone has bundle bone organized in parallel layers with the coronal-apical direction of the tooth and Sharpey's fibres spread obliquely from the lamella of the bone surrounding the socket walls and continuous with the periodontal ligament fibres.

The alveolar bone consists of approximately around 23% inorganic components, 37% organic matrix, and 40% water[17]. The former represents the two-third of the total composition and contains hydroxyapatite crystals, minerals like calcium and phosphate along with hydroxyl, carbonate and citrate and Mg, Na, K, Fl ions. The organic elements consist of cellular components, the osteogenic cells, and matrix made by collagen (primarily Type I) and noncollagenous proteins such as osteocalcin, osteonectin, BMP, Sialoprotein, Phosphoproteins and Proteoglycan[19].

Cellular components

- Osteoblasts: the most active secretory cells in bone, responsible to produce the organic matrix of bone, thus type I collagen and various other noncollagenous bone and plasma proteins. They have a mesenchymal origin and when fully differentiated show a cuboidal or elongated shape that holds a percentage of bony surfaces depending on age and anatomical site. The alveolar bone osteoblasts in the innermost surface of tooth alveolus are arranged to create a suitable accommodation for the Sharpey's fibres inserted into the bone. The periodontal ligament fibres interleave the osteoblasts in the continuous remodeling of the alveolar bone matrix, based on the alternation of temporary detachment of small portions of the periodontal ligament from the alveolus with a new synthesis of the periodontal ligament by fibroblasts and new alveolar bone production by osteoblasts;

this cycle allows the maintenance of tooth biomechanical function[19]. Mature osteoblast may undergo apoptosis, remain bone-lining cells on the bone surface or become osteoclasts, cells encased and surrounded by bone matrix[19,20].

- Osteocytes: osteocytes are stellate cells characterized by a highly dynamic nature. They can remodel in response to physiologic functional forces, guiding the osteoclasts and osteoblasts for bone resorption and formation, respectively. The osteocyte cell size is decreased, the synthetic and secretory organelles are fewer and smaller than osteoblast ones, larger space is occupied by the nucleus but organelles capable for protein secretion are still present. Numerous and extensive cell processes ramify throughout the bone in canaliculi and make contact, frequently via gap junctions, with other osteocytes processes or with the ones extending from osteoblasts or bone-lining cells at the surface of the bone; in this way an essential network of communication is created among these cells, that could suffer from isolation considering the surrounding dense and mineralized matrix[17,20].
- Bone-lining cells: these cells cover the most quiescent bone surface in the adult skeleton and derived from the osteoblasts that undergo gradual morphological and functional changes, till the decrease of protein secretion. They can produce local regulatory substances and modify the composition of the underlying lamina limitans, playing a critical homeostatic role in compartmentalizing the bone matrix and influencing calcium and phosphate metabolism, important in the bone remodeling process. The hemostatic network, made by bone-lining cells and osteocyte processes, regulate plasma calcium concentration in the primary site of mineral ion exchange between blood and adult bone[20].
- Osteoclasts: large and multinucleated cells able to resorb bone in response to biological and functional regulatory factors. They support bony remodeling processes throughout life and mediate bone loss in pathologic conditions by increasing their resorptive activity. Osteoclasts are found on bony surfaces that undergo resorption, in shallow depressions called resorption bays (Howship's lacunae). Their action is mediated by the secretion of hydrochloric acid and proteases, such as cathepsin K, into an extracellular lysozomal compartment beneath a ruffled part of their basal cell membrane to dissolve the mineral and matrix components of bone[19,21].

Matrix components

The extracellular matrix has a composition like other bone tissues, even though the alveolar bone is a specialized structure with specific features and functions. The bone matrix primary components are interwoven collagen fibres with deposits of small and uniform carbonated hydroxyapatite (Ca10[PO4]6[OH]2) crystals. Other proteins, such as proteoglycans, acidic glycosylated and non-glycosylated proteins provide continuity between the matrix and cellular components and the matrix components themselves, regulating the formation of collagen fibres and inorganic crystals[22].

Calcium and phosphate in the form of carbonated apatite (or dahllite) are the predominant inorganic elements that replace the water of the soft, dense connective tissues, like periodontal ligament and gingiva. The organic matrix of bone serves most of the biomechanical function in housing the solid thanks to an ultrastructural organization. This complex structure, consisting of multi-rooted teeth within the alveolar bone, results able to stand the mastication and other unique forces within the oral cavity[19].

- Collagen: It is the major component in mineralized bone tissues. Type I and V collagens, with a percentage of 95 and 5% respectively, assemble the heterotypic fibre bundles responsible for the integrity of the connective tissues. In the alveolar bone, Type III collagen is also found mixed with the type I in Sharpey's fibres, providing a connection with the tooth and probably preventing fibre's mineralization. Besides, also type XII collagen is present and involved in the mechanical strain. Type I, V, XII collagens are produced by osteoblasts, while type III and some of type XII are expressed during the formation of the periodontal ligament by fibroblasts. Intermolecular cross-linking among the collagen fibrils can create a stable structure, providing high tensile strength in the fibres. In the woven (forming) bone, there is a vasty interfibrillar space occupied by mineral crystals since fibres are interwoven. In mature bone, fibres are arranged in layers oriented perpendicular to each other, with little interfibrillar space. In the space between the collagen molecules and channels formed among the regions, crystal formation and growth occur in both the bone[19].
- Noncollagenous proteins: These proteins could change in the various types of bones and show age-related differences in the amounts. Some of them, such as osteocalcin and bone sialoprotein, are essentially unique to mineralized tissues rather than osteonectin/ SPARC (secreted protein, acidic, rich in cysteine) and osteopontin that have a more general distribution. The osteocalcin represents the 15% of noncollagenous proteins in alveolar

bone and it owns a high affinity for mineral bone, attributable to the gla groups of the pro-osteocalcin. Osteopontin plays a role in cell adhesion and several extracellular matrix events involved in the integration between the newer and the older bones during the remodeling cycle. Other noncollagenous proteins secreted by bone cells and plasma-derived proteins, like albumin, a2HS-glycoprotein, immunoglobulins, and matrix gla protein, are also distributed throughout the bone matrix and may compete and/or participate in mineralization processes. Some small proteoglycans such as chondroitin sulfate proteoglycans have specifically modified forms able to interact with mineral crystal through the acidic glycosaminoglycan side of chainsprocollagen peptides. Other proteins, such as thrombospondin, fibronectin and vironectin, can modulate cell attachment and the alkaline phosphatase[14].

Although fundamentally comparable to other bone tissues in the body, alveolar bone is subjected to continual and rapid remodeling associated with teeth eruption and subsequently the functional demands of mastication. Many normal and abnormal processes could cause alterations in maxillary and mandibular bone tissue, such as metabolic and systemic diseases or medical treatments[17]. The ability of alveolar bone to undergo rapid remodeling is also important for positional adaptation of the teeth but may be detrimental to the progression of some illness such as the periodontal disease[23]. This condition can produce noteworthy changes in alveolar bone proper, having significant effects on its function and the ability to repair[18].

When serious inflammations, like pulpitis, affect the tooth, significant alveolar bone loss may also occur[13,18]. Inflammation reactions might involve the periapical part of the root and the PDL adjacent to the apex, leading to an ischemic state and in nonviable and necrotic bone tissue. Untreated dental diseases result in osteolysis that inevitably leads to dental loss[13].

Besides, after tooth extraction, irreversible alveolar bone resorption always occurs, producing dimensional and structural alterations in the alveolar processes of the jaws[24]. Implant installation is the most common functional and aesthetic restoration procedure for missing teeth, but it depends on the quantity and quality of the maxillary or mandibular bone[25].

1.3 Alveolar ridge remodeling after tooth extraction

A dental extraction (or avulsion) is a surgical procedure that involves the removal of a tooth from the dental alveolus (socket), the natural mandibular/maxillary bone cavity in which it is

placed. Extractions are performed when the tooth became unrestorable by conservative methods (e.g., root canal therapy, filling), both for pathological reasons and physical impediments. Severe tooth decay and acute or chronic alveolar infections, such as periapical abscess, are the most common reasons[26,27]. Other critical situations that could lead to the tooth extractions are severe gum diseases, such as the periodontal disease[28] in which tooth supporting tissues and bone structures might be affected, or dental trauma[29], frequently discussed as an etiological factor in the formation of an idiopathic bone cavity[30].

However, even though teeth extractions are common practices in oral surgery, they are often associated with several post-surgical complications, ranged from expected and predictable outcomes, such as bleeding, oedema, infections and alveolar osteitis[31], to more severe and permanent ones[32].

After exodontia, a well-documented sequence of events brings to the alveolar healing. Indeed, immediately after the avulsion, the socket is filled by a blood clot that within 1 week is replaced by granulation tissue. Differently from skin wound healing, epithelial cells migrate over the granulation tissue surface to cover the healing socket because it is recognized as connective tissue. Starting from the apical and lateral residual bony walls, the granulation tissue is rapidly remodeled to provisional matrix; successively mineralizing processes occur, leading to the formation of woven bone that could be also replaced by mature lamellar bone[33]. Notwithstanding this, a lifelong, irreversible and cumulative three-dimensional bone resorption always occurs, mostly during the first year[34]. It starts in concomitance with the healing of the soft and hard tissue wound and continues also after the cessation of *de novo* bone formation into the socket[35]. The bundle bone appears to be the first bone to be rapidly absorbed and replaced with woven bone leading to a great reduction in bony height especially in the buccal aspect of the socket[33].

The amount of bone loss has been estimated at 21% after 3 months, 36% after 6 months, 44% after 12 months, and it seems to proceed at an average of 0.5-1% per year for the entire life[34], resulting in the removal of large amounts of the jaw structure. This remodeling process leads to changes of ridge morphology, mostly in the horizontal dimension but also referred to the vertical ridge height. These changes have been widely described by study cast and cephalometric measurements, radiographic analysis and direct measurements of the ridge following surgical procedures[36]. The key factors cause of these phenomena are still under discussion. On the one hand, the resorption could be a natural consequence of bundle bone

uselessness after tooth removal but, on the other hand, this event could be related to the surgical trauma of the extraction that may imply the separation of the periosteum and its disconnection from the underlying bone surface. In the latter case, vascular damage and acute inflammatory response could occur, mediating bone tissue remodelling[37]. Moreover, local and systemic factors tent to influence the whole healing process and marked differences could also occur between the maxillary and mandible bone[34].

Though, even with uneventful healing following dental extractions, the wound in the extraction socket is only partially restored and alveolar bone resorption leads to the formation of vary-size bony defects[36]. These lesions could also occur as a consequence of periodontal disease if inflammation spreads from gingiva to alveolar bone, trauma, infection secondary to caries, or due to the development of cysts[38,39]

Among all the replacement options, the dental implants are the most common, as well as extremely effective and long-lasting when successfully applied. Some studies report that implants placed immediately after tooth extraction have some advantages such as prevention of bone resorption, reduced number of surgical procedures, and reduction of comprehensive treatment time. However, this procedure is often associated with a residual bone defect between the neck of the implants and residual bone walls[40]. Favorable alveolar ridge architecture and adequate bony volume are essential factors to obtain optimal functional and aesthetic prosthetic reconstructions, thus there are anatomic, metabolic, functional and prosthetic criteria to evaluate, such as the quantity and quality of available bone for dental restoration[36].

1.4 Guided Bone Regeneration and Alveolar Ridge Preservation

To prevent the development of severe bone resorption and provide an adequate bone height and width for successive implant rehabilitation, numerous surgical techniques have been proposed, such as the guided bone regeneration procedures (GBR) and the alveolar ridge preservation (ARP)[41–43].

The GBR techniques lead to lateral and vertical ridge augmentation, aiming to the reconstruction of alveolar bone defects and treatment of peri-implant bone deficiencies, often needed in the absence of ridge preservation; the APR treatments aim to the maintenance of horizontal and vertical ridge dimensions after extraction placing grafting material into the socket to prevent bone resorption and reduce dimensional changes[44,45].

The final goals are[33]:

- Reduction of alveolar bone volume loss.
- Fast bone regeneration and restoration to provide adequate bone volume for implant placement.
- Improvement of the aesthetic outcome of the final prosthesis.

Hence, the rehabilitation of edentulism using osseointegrated implants is a restoration technique that has revolutionized the field of dental surgery and improved patients' quality of life.

GBR, based on the use of membranes and graft materials and aimed at the three-dimensional regeneration of alveolar bone defects[33,46], has become a major treatment option to provide optimal bone support for osseointegrated dental implants. It is based on principles of guided tissue regeneration (GTR), developed by Nyman et al. in 1980, stating that specific cells contribute to the formation of specific tissues[47]. The concept of creating a separated anatomic site in which promote the healing was first introduced when cellulose acetate filters were experimentally used for the regeneration of nerves and tendons[43]. Thus, the biological rationale of GBR is based on the mechanical exclusion of undesirable soft tissues from growing into the osseous defect, allowing only osteogenic cell populations to repopulate the bony wound space[43].

GBR has been used for horizontal and vertical ridge augmentations, demonstrating reliable outcomes with high implant survival rates and low complication rates[48]. The regeneration procedures depend on the migration of pluripotential and osteogenic cells like osteoblasts to bone defect site and the exclusion of cells that obstruct bone formation, non-osteogenic tissue cells like fibroblast or epithelial cells. Osteoblasts could derive from the periosteum, bone marrow and adjacent bone[45]. Thereby, the barrier membranes are essential to refrain gingival cells from penetrating the defect that needs to be regenerated[33].

After GBR procedures, bone regeneration follows a specific sequence of events. Within the first 24 hours after the space underneath the barrier is filled with a blood clot able which releases growth factors (e.g., platelet-derived growth factor) and cytokines (e.g., IL-8) that attract macrophages and neutrophils. Granulation tissue, rich in new blood vessels, replaces the clot allowing nutrients and mesenchymal stem cells capable of osteogenic differentiation to reach the wound site. Woven bone, formed by the mineralization of osteoid, will be the

template for lamellar bone apposition[45]. The optimal healing is presumed to be achieved if the osteogenesis rate extending from adjacent bony margins exceed the fibrinogenesis rate from surrounding soft tissues.

There are four principles to ensure successful GBR: space maintenance, the stability of the fibrin clot, primary wound closure and exclusion of epithelium and connective tissue[49].

The methods that can be used in GBR to enhance the rate of bone formation are the osteoinduction, by the use of appropriate growth factors, the osteoconduction, using grafting material as a scaffold for new bone growth, and the GTR, based on space maintenance by barrier membranes to be filled with new bone[33,45].

Hence, the GBR therapeutic protocol involves the surgical placement of a cell occlusive non-resorbable and absorbable membrane facing the bone surface, to physically seal off the skeletal site in need for regeneration, with or without particulate bone grafts or/and bone substitutes and, more recently, bioactive molecules[46]. The membrane must show suitable characteristics such as biocompatibility, cell-occlusion properties, integration by the host tissues, clinical manageability,

space-making ability, and adequate mechanical and physical properties[48].

Better clinical outcomes are achieved when membranes possess specific properties[50]:

- Ability to exclude from the wound site the gingival fibroblasts or/and epithelial cells, to prevent the formation of fibrous connective tissue.
- Size trimmed to extend about 2-3 mmm beyond all the defect margins so that space beneath it is created when applied; rounded corners prevent flap perforation.
- Ability to protect the fibrin clot from the flap movement during healing to provide the suitable environment to the osteoprogenitor cells; often suture, mini bone screws or bone tracks are used to fix better the membrane.

To support the membrane and prevent its collapse in fenestrations, bone-replacement grafts, serving as an internal framework, or stiffer membranes, such as titanium-reinforced membranes, could be used.

An essential issue in GBR treatment is the membrane, that could be made of different materials or present different modifications[48]. Both non-resorbable and resorbable membrane materials, made by synthetic or natural polymers, have been used in the context of GBR treatment, clinically or experimentally[43].

The most used non-resorbable barriers are the expanded polytetrafluoroethylene (E-PTFE) membranes, representing the first generation of membrane for GBR treatments. E-PTFE is a chemically stable and biologically inert polymer, resistant to microbiological and enzymatic degradation, with a porous and flexible structure and essential space-making capacity[33,43,51].

This membrane is the gold standard of GTR and GBR treatments and consisted of 2 parts: a collar portion, having open pores to allow in-growth of connective tissue and to prevent epithelial migration; and an occlusive portion, preventing the flap tissues from coming into contact with the root surface[50]. Dense-polytetrafluoroethylene (d-PTFE), titanium mesh and titanium-reinforced PTFE are other types of non-resorbable membranes commonly used in GBR procedures[52]. The major drawbacks in the use of non-resorbable membranes are their excessive rigidity and difficult manageability, the necessity of a primary fixation, the increased risk of exposure and increased risk of infection after exposure[52].

To overcome these issues, the second generation of membranes made by resorbable materials was developed and greatly appreciated by patients for the time and cost saved. Collagen type I, polyurethane, polyglactin 910, polyglycolic acid, polyorthoester, polylactic acid and different copolymers of polylactic acid are some of the biodegradable materials tested[48]. Surely collagen keeps the key role among these biomaterials since it is a major component of the bone, acts as a track on which cells can move[50]. Collagen is a haemostatic agent that can stimulate platelet attachment and enhance fibrin linkage, facilitating clot formation and stabilization. Furthermore, it is chemotactic for fibroblasts, easily manipulated and adapted and well tolerated[50].

The resorbable polymers undergo for stages of degradation once placed in an aqueous environment: hydration, strength loss, loss of mass integrity and solubilization via phagocytosis. Nature of polymer, pH, temperature, polymer crystallization degree and membrane volume govern the duration of each stage and the whole degradation rate. The main drawback is related to the high variability in membranes resorption that deeply influences bone regeneration and wound healing processes[43].

The placement of graft materials into a socket has been one of the ARP method proposed to prevent the natural tissue contours at extraction site[42]. Bone grafts substitute materials are also used in the GBR techniques, placing them underneath the membrane to provide structural

support, prevent membrane collapse, preserve the space, and enhance the regenerative capacities of the host tissues.

Physical and chemical properties of graft materials, such as crystallinity, porosity, surface roughness granule size and morphology, influence the performances of the biomaterials from cells behaviour to the bone formation process, playing key roles on the osteointegration and osteoconduction processes.

They are commonly classified in autograft, allograft, xenograft and alloplasts, depending on their origin, although the conventional bone regeneration techniques involve autologous grafts[44].

- Autograft: these types derive directly from the patients, whether oral or extraoral origin and play a key role in bone formation enhancing the osteogenesis by osteoinduction and osteoconduction processes. For ages considered the gold standard of bone grafts, the autograft mechanism is based on two components: the anatomical host site, that provides support for the cellular growth, and the Type I collagen which acts as a pathway for vascularity and neo-angiogenesis. Nevertheless, autogenous bone grafts present some drawbacks such as morbidity of the additional surgical site, limited graft accessibility risk of clinical complication, prolonged operation time and high cost of interventions[45,50].
- Allografts: they derive from individuals of the same species as the host, and are generally classified in frozen bone allograft, freeze-dried bone allograft (FDBA), and demineralized freeze-dried bone allograft (DFDBA). They could have the forms of putties, gels, or particulate (e.g., Puros Cancellous), ready-to-use without the necessity of a secondary surgical site. Although they are a source of type I collagen, they do not provide the bony inorganic calcium whether the scaffolding proprieties to support bone regeneration[45,50].
- Alloplasts: they are inert and synthetic graft materials; hydroxyapatite and calcium phosphate are some exponents of this group. They are used to endure the healing of bony defects and the mechanism of action is strictly osteoconduction. On account on their synthetic origin, they could have different chemical composition, physical forms, and surface configurations (porosity, densities, solubility) that play a key role in the variable level of bioresorbability[45,50].
- Xenografts: materials derived from other species, usually bovine or porcine, deprived of the organic components to avoid the immunological reactions in the host. Thus, they are

inorganic materials rich in calcium and acting as an architectural matrix, able to maintain the augmentation space during the regeneration process. The low resorption rate may negatively impact the healing of the grafted site and compromise the mechanical and biological properties of the regenerated bone[45,50].

Other components used as graft are the recombinant bone morphogenetic proteins (BMP), osteoinductive compounds, and the tissue-derived growth factors for osseous regeneration. About seven BMPs types have shown a speedup of the bone formation process, positively affecting several processes such as chemotaxis, proliferation, and differentiation[50].

A potential solution to provide more predictable results could be the use of bone inductive growth factors that may enhance the development of mature lamellar bone and possibly lead to earlier and more predictable support of dental implants[53].

1.5 Non-transfusional Hemocomponents

In the last years, more reliable and predictable results in the field of regenerative medicine have been obtained using bone inductive growth factors, such as plasma-rich growth factor (PRGF).

The use of blood-derived products on wounds to stimulate healing was first described 40 years ago with the fibrin glues, based on concentrated fibrinogen. Nowadays, autologous fibrin is limitedly used due to the complexity and the cost of their production protocols, thus these products have been replaced by the use of platelet concentrates[54].

Platelet concentrates have been defined as an innovative approach for tissue regeneration, applied in various surgical fields including head and neck surgery, otolaryngology, cardiovascular surgery and, as mentioned before, maxillofacial surgery[55].

The dental and oral surgery applications range from ablative surgical procedures, mandibular reconstruction, and surgical repair of the alveolar cleft to procedures relating to the placement of osseointegrated implants, correlated to the management of post-extraction socket healing.

Autologous platelets-concentrates contain high quantities of key growth factors and cytokines, such as platelet-derived growth factor (PDGF), transforming growth factor-beta (TGF-b), vascular endothelial growth factor (VEGF), and platelet-derived endothelial growth factor (PDEGF), that are released during the plasma-concentrate preparation[56,57]. These factors, also found in tissues during natural healing, have a crucial role in several cell events, like induction, proliferation, differentiation, chemotaxis, and synthesis of the extracellular

matrix that are linked to processes like mitosis, osteoblast proliferation, vascularization, and collagen synthesis[56].

The major effects of these systems are related to the PDGF, important protein for both hard- and soft-tissue healing, able to stimulate chemotaxis, mitogenesis and the replication of stem cells at the wound site. It also promotes the production of hyaluronic acid and fibronectin, a cell adhesion molecule important for cellular proliferation and migration during healing[55,57].

Moreover, TGF-b1 and TGF-b2 are also involved in connective tissue repair and bone regeneration since they can stimulate fibroblast, chemotaxis, the proliferation of mesenchymal stem cells and osteoblasts, and the production of collagen and fibronectin by cells, inhibiting collagen degradation by decreasing proteases and increasing protease inhibitors[55,57].

Thus, the use of platelet-concentrates rich in growth factors in APR and GBR techniques has been considered a promising and innovative strategy to achieve soft and hard tissue healing in the post-extraction sockets[56,58,59] overcoming the drawbacks affecting the traditional procedures. It has been demonstrated that these systems could enhance alveolar bone preservation or regeneration by accelerating bone repair, promoting fibroblast proliferation, and increasing tissue vascularity in the alveolar sockets[55,57]. Improved clinical outcome in terms of percentages of success and reduction of bleeding, inflammation, pain, and discomfort, have been also obtained[57]. Moreover, plasma concentrates are autologous and easily obtained at a relatively affordable cost. They have also demonstrated promising results in the management of extensive periapical lesions, apicomarginal defects, and combined endo-perio lesions[60].

The first generation of blood-derivate products are called Platelet-rich-plasma (PRP) and are obtained by techniques variable in time but all based on collected blood with anticoagulant, just before or during surgery, immediately processed by centrifugation[54].

During the first soft-spin centrifugation step, blood is separated into three layers: red blood cells (RBCs) at the bottom, acellular plasma (platelet-poor plasma, PPP) as the supernatant and a ‘buffy coat’ (BC) layer where platelets are concentrated in between[54] (Figure 2).

The second step for the collection of the “bluffy coat” vary among the different protocols that allow the production of pure PRP (P-PRP) without leucocytes or leucocyte-rich PRP (L-PRP). These two systems production greatly depending on the means of BC collection (Figure 2)[54].

- For P-PRP production, PPP and superficial BC are moved in another tube to undergo hard-spin centrifugation. Discarding most of the PPP layer, the final P-PRP concentrate is obtained and consists of an undetermined fraction of BC rich in platelets suspended in some fibrin-rich plasma but not in leucocytes (Step 2a)[54,58].
- For L-PRP production, PPP, the whole bluffy coat and some residual RBCs are transferred to another tube and undergo hard-spin centrifugation. The final L-PRP is obtained discarding the PPP and consists of the entire BC, rich in platelets and leucocytes[58], and residual RBCs suspended in some fibrin-rich plasma (Step2b).

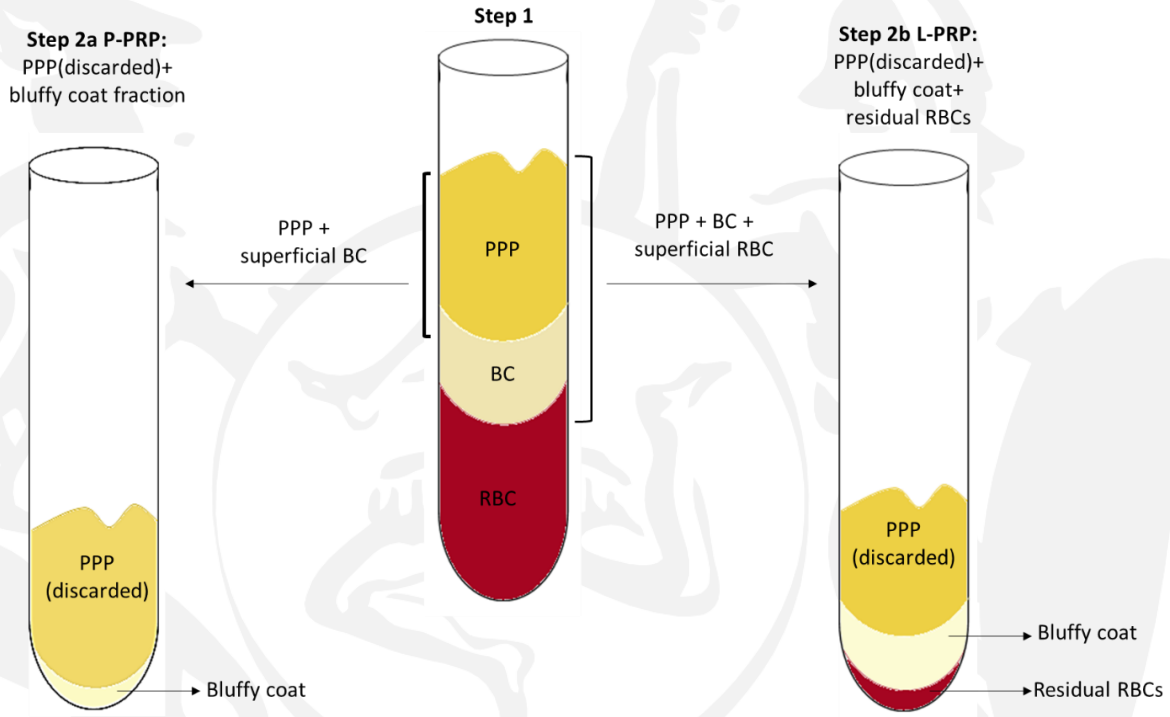

Figure 2: Platelet-rich plasma protocol using a two-step centrifugation procedure.

Finally, whichever is the final product, it is applied by a syringe to the surgical site, together with thrombin and/or calcium chloride (or similar factors) to trigger platelet activation and fibrin polymerization.

The second generation of platelet-derivates has been developed by Choukroun et al. and are the platelet-rich fibrin (PRF), obtained from collected blood without any anticoagulant and immediately centrifuged[27,61]. The formation of leucocytes and platelet-rich fibrin (L-PRF) occurs following a natural coagulation process, that does not require biochemical

modification of the blood, any anticoagulant, thrombin, or calcium chloride. The easy and not expensive protocol is surely the advantages of this open-access technique[61].

A clear classification of platelet concentrates is possible following three main parameter sets[54]:

The first is related to the preparation kits and centrifuge machine used. In particular, the centrifuge size, duration of the procedure, costs of kits and devices and procedure complexity are important factors, since they own a significant impact on the daily use of these surgical techniques.

The second group of parameters relates to concentrating content. Indeed, the final volume of usable concentrate influence the potential clinical applications of the preparation protocol and deeply depends on the initial blood harvest. The efficiency in collecting platelets and leucocytes and their preservation during the process are the other three parameters that tend to influence the pharmacological relevance and potential applications of the products.

The third set of parameters are related to the fibrin network supporting platelets and leucocytes concentrates during the application. Fibrin network density plays a key role and is mainly determined by fibrinogen concentration during preparation. Low-density fibrin networks allow convenient surgical application, but true fibrin support matrix is missing, while high-density ones could be considered as biomaterials owing potential healing effects itself.

Another important parameter is the fibrin polymerization process that relates to fibrinogen and thrombin ratios, correlated to the biomechanical properties of the final fibrin network since thrombin actives fibrinogen which polymerizate into fibrin. Fibrin fibrillae can be organized in two biochemical architectures, either as condensed tetramolecular or bilateral junctions or as connected trimolecular or equilateral junctions. The former derives from a drastic activation and polymerization, that could happen with high thrombin concentrations that lead to the formation of a dense network of monofibres, not suitable for cytokine enmeshment and cellular migration. Instead, the equilateral junctions derived from a slow physiological polymerization that leads to the formation of a flexible fibrin network with multifibres, with elasticity similar to that of a solid biomaterial and able to provide the adequate support for cytokine enmeshment and cellular migration[54].

1.6 L-PRF and PRF-Block

Leucocyte-and platelet-rich fibrin is the second generation of platelet concentrated, obtained by a simple and free technique developed in France by Choukroun et al.[62] in 2001 without any anticoagulants or gelifying agents[63].

The protocol developed by ©2018 Intra-Lock International, the partner company of the PhD project, was followed to create the L-PRF and its derivate, the PRF-Block.

This preparation method involves the collection of venous blood in a dry glass tube and the low-speed centrifugation during which, in absence of anticoagulants, fibrin polymerization and platelet activation are triggered immediately. Three layers are formed after centrifugation: the RBCs at the bottom of the tube, acellular plasma top layer (both discharged) and a PRF clot in the middle (figure 5)[54,61].

Both platelets and leucocytes are collected with high efficiency, preserving the leucocytes throughout the entire process and, platelet activation during the procedure leads to a substantial embedding of platelet and leukocyte growth factors into the fibrin matrix[54,61,63].

Indeed, the L-PRF clot is a strong fibrin matrix characterized by a complex three-dimensional architecture rich in platelet and leucocytes that, if pressed between two gauzes, could become a strong membrane (Figure 3) and widely applied as an autologous biomaterial in oral, maxillofacial, ENT (ear, nose, throat) and plastic surgery[63,64].

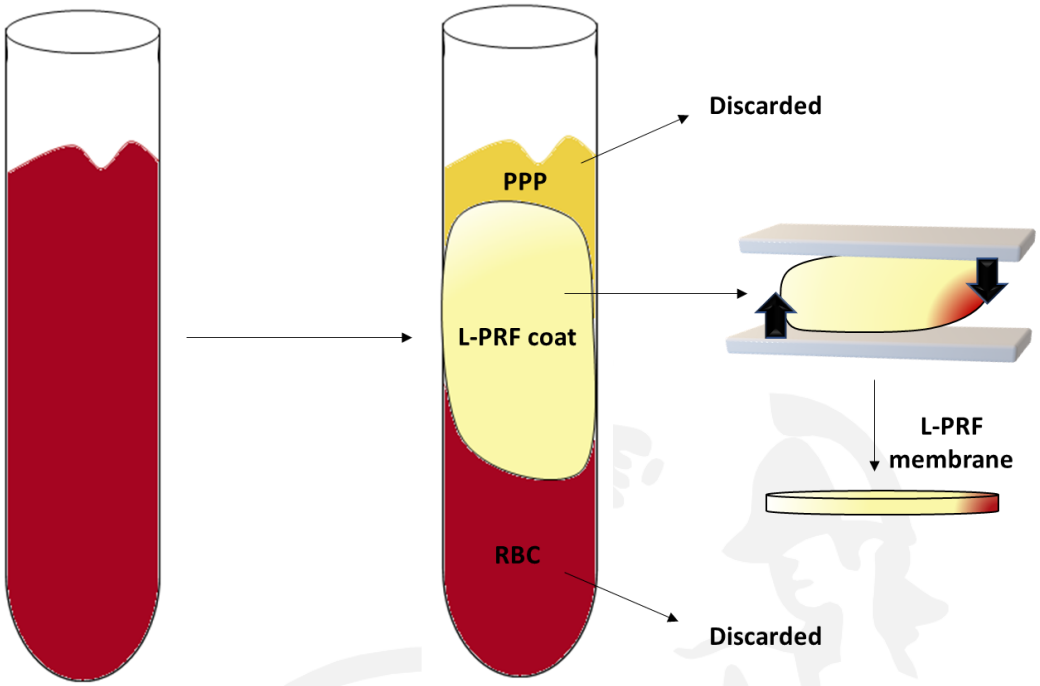

Figure 3: L-PRF clot obtained from collected blood without anticoagulants and compressed to obtain L-PRF membrane.

As the other platelets derivate, its use leads to an improvement of soft tissue healing[63] and bone graft protection and remodeling but, in contrast with PRPs, PRF does not dissolve promptly once applied in the target site, instead it undergoes slowly remodeling like the natural blood clots[54].

The growth factors and cytokines are released from the L-PRF in a continuous and delayed manner, most significant in the early days but sustained up to 21 days[64]. Their action is mostly related to the regulation of the inflammatory process and increases angiogenesis, allowing speeding up the tissue healing process. Furthermore, fibrin-based scaffolds are considered biomaterials able to provide physical support for different cells such as neutrophils, macrophages and fibroblasts, which will produce collagen, fibronectin and other extracellular matrix components[65].

Several medical disciplines have used L-PRF in different types of surgery, including periodontology, implant dentistry, and maxillofacial surgery, reporting a positive effect for the wound healing process. Actually, L-PRF dense plugs or membranes can be adapted to several tissue defects, as in case of post-extraction sockets and have been used in ARP and, recently, in GBR procedure[30,56,66,67].

Several studies on alveolar sockets preservation have underlined that sockets treated with L-PRF as "sole" grafting exhibited a faster wound healing after tooth extraction, compared to the natural and spontaneous healing and similar results in ARP as other bone substitutes, with several advantages such as simplified procedures, less post-operatory pain and inflammation, the absence of residual graft particles, and the benefit of its low cost[58,59].

The fast epithelization of alveolar soft tissue might also reduce the possibility of complications, such as osteitis and postoperative pain, and the preservation of alveolar bone may promote osseointegration and improving implant stability, leading to reliable and successful functional restoration by implants[67].

An interesting L-PRF derivate is the Platelet Rich Fibrin Block (PRF block), obtained combining L-PRF membranes, Liquid Fibrinogen and bone graft materials, and resulting in a strong construct of fibrin integrating the bone substitute[65] (Figure 4).

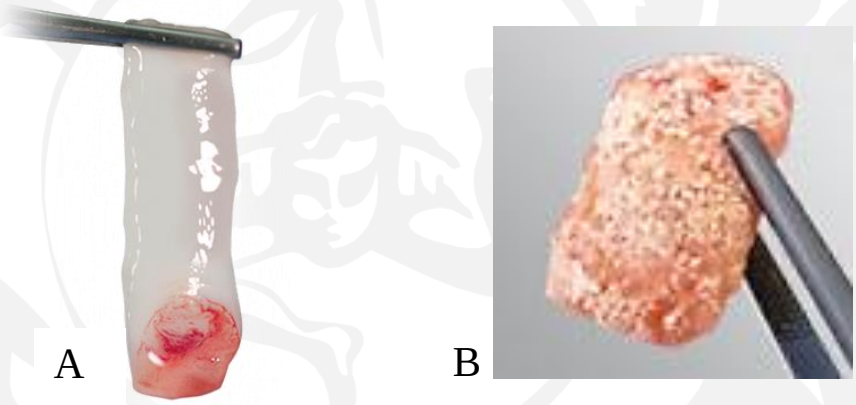

Figure 4: A) L-PRF clot; B) PRF-Block

This putty form of L-PRF is obtained mixing the cut L-PRF membranes and the graft materials with Liquid fibrinogen, that acts as a clotting accelerator for the L-PRF/Biomaterial. The adaptation and healing qualities of the bone graft will be enhanced by its hydration with the L-PRF compression exudate, that helps create the desired putty-like consistency. In this way, the biomaterial is captured in the fibrin matrix and coagulated using the liquid fibrinogen, increasing the biomaterials handling & biologic capacity.

Although the PRF-Block has a recent development, it has already exhibited promising results both in ARP and GBR procedures. Indeed, if desired, PRF-block could be applied directly

into the defect site, that after could be closed by L-PRF membranes[66]. The promising aspect of PRF is based on the combination of the xenograft, acting as a scaffold with osteoconductive ability, and the L-PRF membranes serving as a bioactive nodule with osteoinductive capacity[65].

b) Technological approach for tissue regeneration

Factors such as microbial infections, presence of excessive free radicals and reduction in antioxidant-based scavenging systems cause serious challenges by prolonging inflammation and delaying bone repair processes[68]. For these grounds, the employment of scaffold or nanocomposite enriched with antimicrobic and antioxidant agents is considered as a promising tool for bone regeneration bioengineering.

As mentioned above, resorption of the alveolar ridges and consequently bone loss is in both vertical and horizontal dimensions always occur after tooth extraction. However, bone remodeling and reabsorption can also occur before teeth extraction, as a consequence of oral diseases as periapical pathology, periodontal disease or trauma to teeth and bone[36,69]. In some of these conditions, one of the major causes for delay or failure in the bone restoration process is the infection, thus the use of antibiotics could improve the bone healing process[70].

Metronidazole (MTZ) is an antibiotic from the nitro-5-imidazole family used in the periodontal disease treatment since its action against anaerobic organisms, strongly associated with the damage of periodontal tissue[70] (Figure 5). However, its systemic administration is associated to several side effects, such as hypersensitivity and gastrointestinal intolerance, drawbacks related to the gastrointestinal tract, such as diarrhoea, nausea, vomiting, and pseudomembranous colitis and its prolonged use tent to increase the risk to develop a bacterial resistance[71,72].

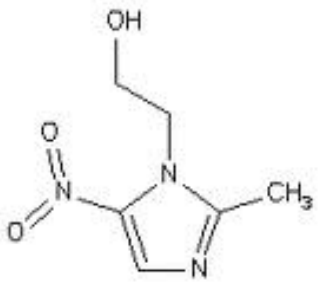

Figure 5: MTZ chemical structure

Bone reabsorption could be also promoted by an overproduction of reactive oxygen species (ROS) and, subsequently, oxidative stress not balanced by antioxidants. The main consequences are a reduction of the wound healing process and altered bone metabolism due to increased differentiation of preosteoclasts in osteoclasts[73]. Thus, bone recovery could

benefit from the use of antioxidant agents such as Curcumin (CUR), a polyphenolic compound known for a wide variety of biological activities such as antioxidant, antimicrobial, anti-inflammatory, anti-arthritic and chemopreventive properties commonly applied in dentistry[74,75] (Figure 6).

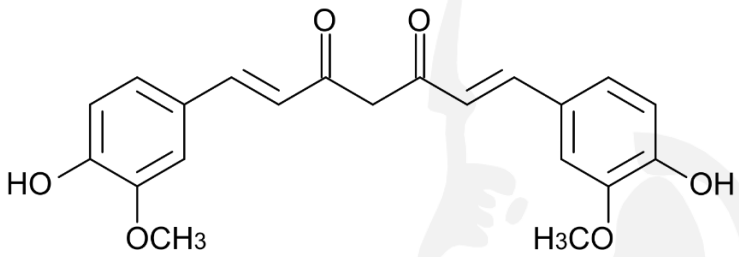

Figure 6: CUR chemical structure

It has been demonstrated that a topical administration of CUR in the post-extraction socket right after the surgical treatment can decrease soft tissue inflammation, can protect the wound from bacterial infections, increase collagen deposition and stimulate cell proliferation, improving tissue regeneration[76]. However, CUR is characterized from an extreme lipophilic nature and physicochemical instability, thus it needs to be loaded into the pharmaceutical formulation to be available in aqueous environment[77], and among the numerous carrier strategies, lipid-based colloidal dispersions seems to be suitable to overcome the problems of degradation, poor solubility, and penetration inside the tissue[78,79].

In the last years, the interest in lipid nanoparticulate systems has increased mainly due to their versatile nature as controlled release systems for lipophilic compounds.

The nanoscale dimensions associated with a large surface to volume ratio, comparable to peptides and small proteins, allow nanoparticles diffusing across membranes and facilitate uptake by cells, mimic the natural nanometer size scale of the extracellular matrix (ECM) components[80]. Since classic engineered materials used in tissue engineering are not always able to mimic the natural properties of the target tissue and to overcome this drawback, the development of customized nanoparticles could be a solution.

The first generation of lipid nanoparticles is represented by the solid lipid nanoparticles (SLNs), developed in early 1990 to match the advantages of colloidal systems with high biocompatibility and the biodegradability of the lipid constituents. The SLN preparation

requires the use of a single solid lipid and surfactants, that could vary from soy lecithin, polysorbates to Pluronic.

The advantages of using SLN as modified release systems are numerous[81]:

- Ability to control drug release
- Increased drug stability
- A decrease in the volume of drug distribution
- Absence of carrier toxicity
- Absence of organic solvents in the preparation phase
- Possibility of large-scale production and sterilization
- A wide spectrum of applications
- Possibility of active targeting functionalizing the surface.

However, SLN main drawback is the low drug loading capacity, related to the tendency to expel it over time and attributable to the uni-lipid composition of SLNs. Indeed, the lipid tents to undergo polymorphic transitions, from metastable to stable form till the formation of highly ordered structure, that means the decreasing of available space for the entrapped substances, which are expelled[82].

A natural evolution of SLNs is represented by nanostructured lipid carriers (NLC), the new generation of lipid nanoparticles developed to overcome the loading problems associated with SLNs (Figure 7).

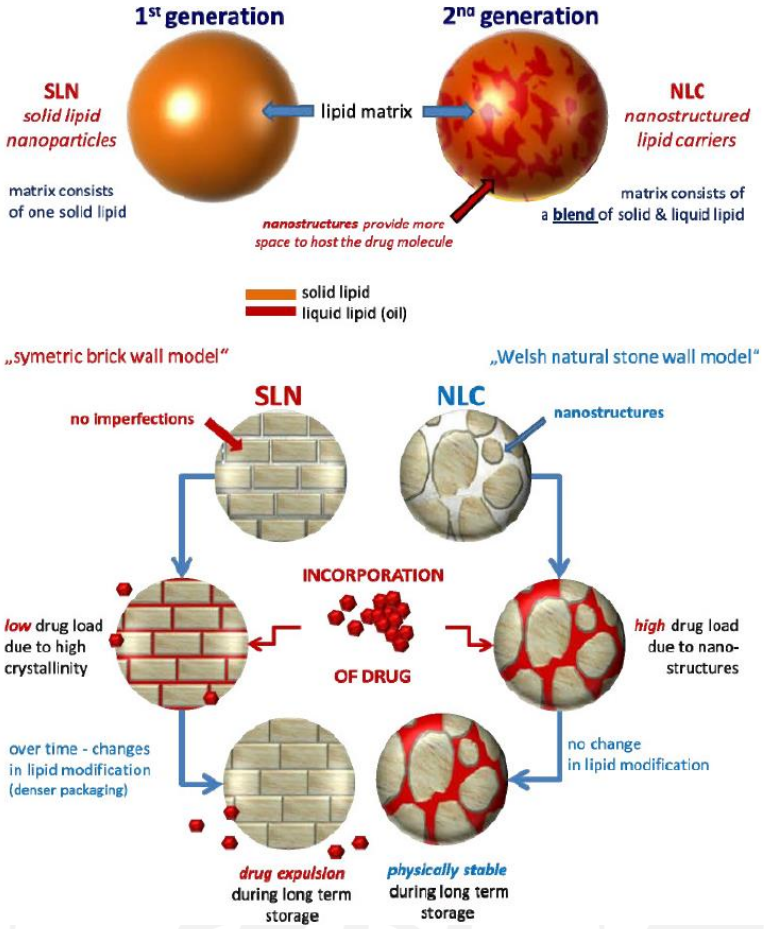

Figure 7: Differences between SLNs and NLCs[83]

NLCs are composed of a mixture of biocompatible and biodegradable liquid and solid lipids with short and long chains, mainly mono-, di- and triacylglycerides, fatty acids and waxes, that provides the system the ability to load great amounts of drug since the system is composed of an amorphous and highly disordered structure. Moreover, the imperfect architecture of the lipid matrix plays a key role in the controlled release phenomena, owed to the slowly and gradually phase transition that lipids undergo once in contact with the mucosae, that allow avoiding the burst effect typical of SLN[83].

Recently, sponges, defined as a dispersion of gas in a solid matrix with a porous structure, have been developed as an innovative formulation for the design of wound dressing and transmucosal drug delivery systems. They are prepared by removing water from a polymer matrix by a freeze-drying procedure to obtain a solid, dried, soft, and flexible structure in which NLCs could also be entrapped[84–86], obtaining a nanocomposite biomaterials.

In the light of previous considerations, the use of both antioxidant and antimicrobial agents could be an interesting approach to enhance bone preservation or restoration in the post-extraction socket. Thus, an innovative and promising strategy could be the development of multi-composite biomaterials and scaffolds consisting of sponges loaded with antimicrobial agents and nanostructured lipid carriers containing lipophilic antioxidant, to be applied in association with the L-PRF and deliver the actives on surgical sites of teeth extractions. This innovative approach could promote ridge preservation, prevent bone reabsorption and support bone regeneration[87].

Aim of the PhD thesis

This PhD thesis is based on a project cohering with the National Operational Program (PON) "Research and Innovation" (R&I) 2014-2020 funding by the Italian Ministry of Education, University and Research.

The project is focused on the development and promotion of Regenerative Medicine to improve the oral health-related quality of life of patients in need of implant-based rehabilitation after tooth extraction. As part of this program, the aim of this thesis was the validation of an innovative protocol for the Guided Bone Regeneration using the second generation of autologous platelet concentrate, the Leukocytes and Platelet-rich Fibrin (L-PRF), to prevent alveolar bone resorption and promote bone regeneration in the post-extraction sockets.

The L-PRF was obtained following the ©2018 Intra-Lock International protocol, thus withdrawing and processing the patient's blood, and has been applied in the post-extraction sockets as L-PRF membrane or PRF-Block. Their ability to prevent alveolar bone resorption and ridge dimension variations and to promote soft tissue healing and bone regeneration in size-variable bony defects were evaluated.

This innovative procedure has been developed to overcome the drawbacks related to the conventional GBR procedures, based on the use of external membranes and bone substituted from different sources and it is founded on the know-how of the partner company in standardizing the preparation method of L-PRF and PRF-Block combining with the expertise of oral surgeons of the University of Palermo.

The interest in the use of L-PRF and PRF-Block in bone regeneration is constantly arising among the oral researchers, but, since it has been only recently investigated, the collected results are still limited. Within this context, the outcomes achieved by this study appear to be in line with contemporary literature proving an added value at the same.

Moreover, several complications can occur after dental avulsions due to the establishment of local inflammatory processes, as well as the onset of microbial infections, mainly generated by bacteria Gram-negative.

Thus, the secondary aim of this PhD thesis was the development and the characterization of a nanocomposite biomaterial consisting of a hyaluronate-based sponge loaded with

metronidazole (MTR) and nanostructured lipid carriers containing curcumin (CUR-NLC) able to release the actives on post-extractive socket.

Indeed, curcumin is a natural compound owing interesting properties, such as antioxidant, anti-inflammatory and antibacterial, but it is characterized by pronounced lipophilicity, poor solubility in aqueous media and high environment chemical instability. Thus, to promote the absorption of this poorly soluble active ingredient through the tissues of the oral cavity, suitable nanostructured lipid carriers have been designed as delivery system.

Furthermore, bacteriological studies have shown that most forms of periodontal disease are infections caused by excessive growth of a limited number of Gram-negative and anaerobic microorganisms and Metronidazole is the ideal antibiotic for these types of infections.

Since this nanocomposite has been designed to be applied wrapped in the L-PRF membrane, minitablets need to be prepared, to obtain standard systems with suitable dimensions for the post-extraction sockets.

The application of this innovative system after tooth extraction may be able to promote the process of tissue regeneration due to the anti-inflammatory and antioxidant properties of Curcumin, and the antibacterial properties of Metronidazole, supporting and enhancing L-PRF application in dental and oral fields.

CHAPTER 2

Materials and Methods

a) Leucocytes and Platelet rich Fibrin(L-PRF) for Guided Bone Regeneration and Alveolar Ridge Preservation

2.1 Patients characteristics

This study was designed to evaluate the outcomes of solo L-PRF and L-PRF and PRF-Block in patients in need of bone augmentation or preservation before implant placements.

A total of 15 patients in need of tooth extraction in the mandible or maxilla and schedule for future implant rehabilitation were enrolled at the Unit of Oral Medicine of the University Hospital (Policlinico Paolo Giaccone, Palermo) between May 2018 and May 2020.

The study adhered to the principles described in the Declaration of Helsinki and began after the approval by Ethics Committee of the University Hospital "Policlinico Paolo Giaccone" in Palermo (approval number 09/2018).

Before the surgical practices, all patients were informed of the study's procedures/ objectives and signed written informed consent.

The patients were divided into two groups, depending on type of lesion, and required treatment.

GBR group: Five patients were treated by GBR techniques after dental avulsion to regenerate three-dimensional bone defects, often attributable to vast periapical cysts; one patient was affected by a critical-size bone defect. L-PRF and PRF-Block were used in combination in all the surgical treatments.

ARP Group: Ten patients were treated by ARP procedures to prevent alveolar bone resorption, in need of tooth extractions for excessive dental mobility due to extensive caries with endodontic/periapical involvement. Only L-PRF was used in five of those patients; L-PRF and PRF-Block were used for the remaining ones.

The demographic characteristics of patients are reported in table 1.

Table 1: Patient characteristics

Gender	Male	6
	Female	9
Age	Mean	49.4
	Range	29-70
Tooth site location	Incisor	2
	Canine	2
	Premolar	5
	Molar	12
Reason for tooth extraction	Periodontal	8
	Crown fracture	1
	Cyst	6

2.2 Inclusion and exclusion criteria

The patients fulfilled the following inclusion criteria:

- older than 18 years
- no medical history that contraindicates the surgical procedure
- healthy or with systemic disorders (e.g., diabetes mellitus, clotting and osteometabolic disorders) suffering from horizontal, vertical, or combined bone atrophies
- healthy or with systemic disorders (e.g., diabetes mellitus, clotting and osteometabolic disorders) requiring oral surgery to remove dentary elements in bone inclusion or maxillary bone cysts and contextual regenerative bone procedures and with a high risk of post-operative complications

A patient was excluded in the presence of any of the following contraindication:

- pregnancy
- heavy smokers ($\geq$ 15 cigarettes *die*)
- under antiresorptive therapy (as bisphosphonates) for more than 3 years
- cancer disease and radiant therapy of the head-neck district

- conditions as decompensated diabetes, decompensated metabolic and hematologic diseases and ASA IV patients.

2.3 Preparation of L-PRF and PRF-Block

Before the beginning of the surgical procedures, L-PRF and PRF block were prepared according to the techniques described by Dohan et al. (2009)[54] and Cortellini et al. (2018)[66] and the Intra-lock protocol. The whole preparation is shown in figure 8.

Protocol for preparation of L-PRF

- Collection of 8 tubes of venous blood (about 10 ml each) from patients; withdraws must be carried out as quickly as possible because no anticoagulant is present in the tube and blood starts to clot in about 2 minutes. Two tubes with the white cap and glass coating (WCT; IntraSpin™, Intra-Lock, FL, USA) and 6 tubes with the red cap and plastic coated (BVBCTP2; IntraSpin™, Intra-Lock, FL, USA) were used.
- Centrifugation in the IntraSpin™ system (ISS220 Intra-Lock, FL, USA) at 2700 rpm.
- After 3 minutes, interrupt the centrifugation to remove the two white cap tubes.
- Immediately restart the centrifuge with red cap tubes for other 9 minutes.
- Aspirate with a sterile syringe the Liquid Fibrinogen (PLyF), the yellow supernatant of white cup tubes, getting as close as possible to the red cells being attention to not aspirate them.
- After full centrifugation, three layers were formed in the red cap tubes: a base of red blood cells at the bottom, acellular plasma on the top (supernatant), and a clot of PRF between them.
- Withdraw the L-PRF clots by sterile tweezers and isolated from the RBCs.
- Discard the RBCs and PPP.
- Obtain the L-PRF membrane moving the clots on the grill of the Xpression Box (IntraSpin™, Intra-Lock, FL, USA) and press for about 5 minutes.
- Collect the exudate for next steps.

Preparation of "block"

- Chop from two to three L-PRF membranes into small pieces and mix in Ti-dish to 0.5 g of β-tri-Calcium phosphate (Sint-Oss, Industrie Biomediche e Farmaceutiche srl, SA, Italy) (50:50 ratio).
- Add L-PRF exudate if the mix is too dry.
- Spray 1cc of liquid fibrinogen and stir gently for ±10 s and shape to obtain a homogeneous complex with the desired form.
- The activated platelets of the chopped membranes let fibrinogen to polymerize into fibrin within few minutes, entrapping the biomaterial into a fibrin network containing platelets and leucocyte.

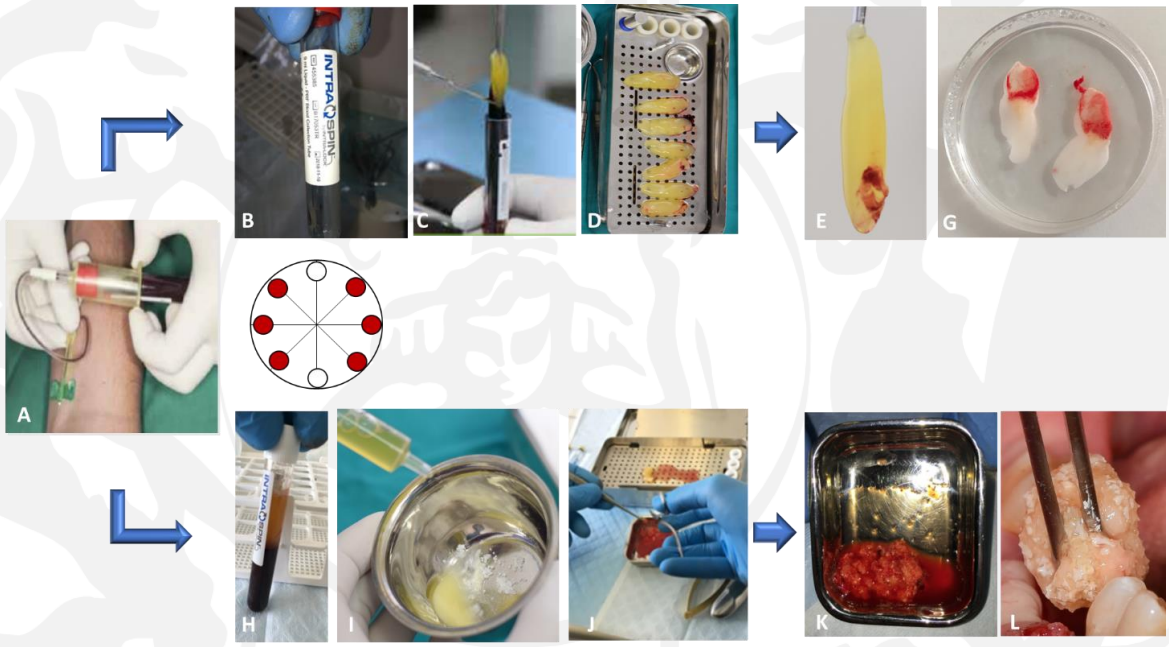

Figure 8: L-PRF and PRF-Block preparation: A) Blood collection; B) Red cup tube; C) L-PRF clot formation after 12 min centrifugation at 2700 rpm; D) Clots on the grill of the Xpression Box; E) G) L-PRF membranes; H) White cup tube; I) J) PRF-Block formation; K) L) PRF-Block.

2.4 Treatment procedures

To assess the absolute requirement for the dental extraction, all the patients underwent clinical examination, intraoral radiographs and, when required, computer tomography scan (CT/CBCT).

These assessments allowed evaluating the alveolar bone conditions and the presence and dimensions of bony lesions, defining the need for GBR or ARP procedures.

When necessary, antibiotics (amoxicillin + clavulanic acid 500/125 mg) were prescribed for 7 days.

Before exodontia, a periodontal treatment, based on plaque control and supra and subgingival scaling, was performed on all the participants, that also received 30mL of chlorhexidine 0.2% mouthwash to swish up for 60 s. Then, local anesthesia was achieved using 3% mepivacaine hydrochloride with adrenaline.

2.5 GBR procedures

- Performance of a full-thickness midcrestal incision between the teeth preserving the interdental papilla and two full-thickness vertical incisions down to the bone on either side.
- Elevation of a full thickness mucoperiosteal flap.
- For teeth in need of extraction, tooth luxation and extraction, gently performed with elevators and forceps and minimally traumatic procedure.
- Removal of cysts when present and debridement of the post-extraction sockets from granulation tissue, performed by miller surgical curette (Figure 10a, b).
- Cortical perforations made with a round bur in the buccal cortex.
- Performance of perioplastic surgery.
- Application of L-PRF clot under the sinus floor and L-PRF block in the bone lesion and post-extraction sockets (Figure 10c).
- Application of the remaining L-PRF clots over the surgical site (Figure 10d, e).
- Tension-free soft tissue closure (Figure 10f).
- Removal of suture after 7-10 days.

2.6 ARP procedures

- Dental luxation and extraction performed with elevators and forceps with minimally traumatic procedure.
- Revision of the socket and irrigation with sterile saline solution.
- Application of just L-PRF or L-PRF block in the alveolus.
- Application L-PRF membrane clots over the surgical site.
- Graft stabilization by sutures.
- Removal of suture after 7-10 days.

2.8 Postoperative control, follow-up, and implant placement

Analgesics (600 mg ibuprofen) were prescribed every 6 h in case of pain. In the following weeks, patients were under strict oral hygiene measures and were seen for the postoperative appointments at seven-ten to value the presence of infections or swelling and the healing of the soft tissue. Further controls were assessed after one, three and six months.

In case of uneventful tissue healings and when require, implant placement was performed six months after the exodontia. The gums were sewed shut over the implant, and sutures were removed after 7-10 days. When required, above all in patients presenting periapical cysts, alveolar bone samples were collected using trephine bar before implant surgery.

Three months after the placement, clinical and radiographic evaluations and implant retained provisional restorations were performed. The definitive implants were loaded after about two months once bone tissue regeneration was achieved and estimated as well as implant osteointegration in *de novo* bone.

2.9 Clinical measurements

Once sutures have been removed, 7-10 days after extraction treatment, the aspect of soft tissue was evaluated.

The soft tissue healing was assessed based on modified healing index of Landry et al[67]. The parameters used to assess the level of healing were the color of tissue, the epithelialization of wound margins, the presence of bleeding on palpation, and granulation.

Following these criteria, the healing level was scored as very poor, poor, good, very good, or excellent (Table 2). This evaluation was performed by an experienced professional and calibration was done before the study.

Table 2 Criteria (Landry et al., 1998) for the soft tissue healing assessment.

CRITERIA	HEALING INDEX				
	Very poor ***1***	***Poor*** ***2***	***Good*** ***3***	***Very good*** ***4***	***Excellent*** ***5***
TISSUE COLOUR	more than 50% of gingivae red	more than 50% of gingivae red	less than 50% of gingivae red	less than 25% of gingivae red	all gingivae pink
RESPONSE TO PALPATION	bleeding	bleeding	no bleeding	no bleeding	no bleeding
GRANULATION TISSUE	present	present	none	none	none
INCISION MARGIN	not epithelialized with loss of epithelium beyond margins	not epithelialized with connective tissue exposed	no connective tissue exposed	no connective tissue exposed	no connective tissue exposed

2.10 Radiographic measurements

Bone healing, augmentation and regeneration were determined by radiographic measurements considering the variations in bone volume and density.

Dental radiographs and cone-beam computed tomography (CBCT) were acquired pre-operatively to value the eventual presence and size of cysts and six months after treatment to confirm the bone regeneration following GRB procedures and the maintenance of the adequate bone volume as results of ARP treatments.

Besides, a dental radiograph was also performed three months after implant placement to verify the osteointegration and implants parameters, such as absence of radiolucent interface between bone and implant and peri-implant bone loss, have been also valued.

2.11 Materials

Curcumin was purchased from Alfa Aesar (Karlsruhe, Germany), isopropyl palmitate (IP), glycyrrhetic acid (GA), sodium hyaluronate (HyNa), and metronidazole from A.C.E.F S.p.a. (Fiorenzuola d'Arda, Italia) and Isopropyl myristate (IM) and Polysorbate 20 from Farmalabor, Canosa di Puglia, Italy. 1-hexadecanol (HEXA), Tween 80 (Tw80), Pluronic F-68 (P-68), and polyvinylpyrrolidone (PVP-K90) were from Sigma Aldrich (Saint Louis, MO, USA), and Trehalose dihydrate (TRH) from la Hayashibara Shoji (Okayama Japan).

Citrate buffer 10 mM (pH 6.2) was obtained dissolving 2.675 g of sodium citrate dehydrate and 0.190 g of citric acid monohydrate in 1 L of distilled water.

Non-enzymatic artificial plasma pH 7.4 (PBS) was prepared dissolving 2.80 g of KH_2PO_4 and 20.5 g of Na_2HPO_4 in1 L of distilled water, with or without the 4% of Polysorbate 20.

Buffer pH 6.8 solution simulating saliva was prepared using NaCl (0.126 g), KCl (0.937 g), $NaHCO_3$ (0.631 g), KSCN (0.655 g), KH_2PO_4 (0.2 g), Urea (0.2 g), Na_2SO_4 (0.154 g), NH_4Cl (0.178 g), $CaCl_2$ (0.130 g), and $NaHCO_3$ (0.631 g) in distilled water; 0.9% saline solution was prepared by dissolving 9 g of NaCl in 1 L of distilled water.

All chemicals and solvents of analytical grade were purchased from VWR International (Milano, Italy) and used without further purification.

2.12 Lipid ratio mixtures screening studies

Lipid mixtures (LM) made by HEXA, IP, and GA were prepared changing both the ratio of the components and CUR (Table 5). 50 or 80 mg of CUR were added under stirring to 950 or 920 mg of pre-heated at 70°C LM by a silicon bath on a hot plate (Heidolph MR2001 K equipped with EKT 3001 electronic temperature control, Germany) and samples were maintained in these conditions for one hour. The lipid mixture considered good was cooled at room temperature and finally stored at 2-4°C until the subsequent use. After 24 hours, the melting point of the mixture was evaluated (Büchi Melting Point B-540). The analysis was carried out in triplicate and the results were expressed as the mean of the values obtained.

2.13 Preparation of CUR-Loaded NLC and CUR-Loaded NLC Dispersion Enriched in Metronidazole

MIX7 was chosen to prepare the CUR loaded NLCs, by the homogenization followed by probe sonication method. Briefly, 20 mL of 10 mM citrate buffer pH 6.2 containing 1% (w/v) Tw80 and/or 1% (w/v) F-68, previously brought to 90 °C, were added to the melted lipid mixture (100, 200, or 300 mg) and firstly homogenized at 30,000 rpm (Polytron Model PT MR 2100, Kinematica, Switzerland) for 1 min and then sonicated by an ultrasonic homogenizer SONOPULS (Bandelin, mod. HD 2070) for 10 min in pulsatile mode with cycles of 0.7 s of activity and 0.3 s of inactivity. Then an additional ultrasonic treatment of 10 min was carried out, placing the container in an ice bath. The compositions of the prepared NLCs are given in Table 6.

M7-300-TP dispersion was chosen for the next step. 150 mg of MTZ were solubilized in 20 mL of hot 10 mM citrate buffer pH 6.2 containing the surfactants before the CUR-NLC preparation. Therefore, the CUR-NLC with MTR dispersion (CURNLC-MTR) was prepared in the same way as previously described.

2.14 Characterization of Nanostructured Lipid Carriers

2.14.1 Particle Size, Polydispersity Index, and Zeta Potential Analysis

The mean particle size, the polydispersity index (PI), and the zeta potential (ZP) were determined by dynamic light scattering (DLS) using a Nano-ZS Zetasizer (Malvern Instruments, Worcestershire, UK). All experiments were performed at 25 °C under an electrical field of 40 V7 cm for ZP analyses on the day NLCs were prepared. The results of all NLCs analyzed are reported in Table 7.

2.14.2 Morphology by Scanning Electron Microscopy (SEM) and Transmission Electron Microscopy (TEM)

To evaluate the morphology and the topographic characteristics of both CURNLC-MTR and CUR-NLC dispersions, SEM analyses were performed. Measurements were carried out using a scanning electron microscope (Zeiss EVO MA10, Oberkochen Germany) equipped with an SE-Everhart-Thornley secondary electron detector with lanthanum hexaboride (LaB6) cathode as the source of electrons, an accelerating voltage of 20 keV and probe voltage of 10 pA and the scanning electron microphotographs were acquired in high-vacuum condition and magnified up to ×50.000 (200 nm).

Few drops of fresh CUR-NLC dispersion were put on an aluminum stub, placed in a $CaCl_2$ desiccator at 8°C for 24 h, and then coated with an ultrathin layer of gold (thickness about 2 nm), to increase the surface electrical conductivity. For the samples of sponges loaded with MTR and CUR-NLC, a gold coating was applied before each analysis.

For the TEM measurements, one drop of diluted CUR-NLCs and CURNLC-MTR was placed on a carbon-coated 200 mesh copper grids for 5 min and negatively stained with 1% uranyl acetate solution before being allowed to dry, and the samples were visualized by using a JEOL JEM-1011 microscope (JEOL Ltd., Tokyo, Japan) equipped with a tungsten thermionic gun operating at 100 kV accelerating voltage. The TEM images were acquired with an 11 MPx Orius 1000 CCD camera (Gatan, Pleasanton, CA, USA).

2.14.3 Entrapment Efficacy (EE) of NLC

The total amounts of CUR and MTR in the fresh NLC dispersion were determined by UV-Vis. Thus, the drug recovery (DR) was determined and calculated by the following Equation (1):

$$DR\%\left(\frac{W}{W}\right) = \frac{\textbf{Drug in formulation}}{\textbf{Drug used}} \times 100 \quad (1)$$

Then, entrapment efficacy (EE) and loading capacity (LC) of NLCs were indirectly determined by quantification of free CUR (unentrapped) in the aqueous medium, applying respectively Equations (2) and (3)[88]

$$EE\%\left(\frac{W}{W}\right) = \frac{\textbf{CUR in formulation} - \textbf{free CUR}}{\textbf{CUR in formulation}} \times 100 \quad (2)$$

$$LC\%\left(\frac{W}{W}\right) = \frac{\textit{CUR in formulation} - \textit{free CUR}}{\textit{Lipids amount}} \times 100 \quad (3)$$

To evaluate the concentration of the unentrapped drug in the aqueous medium, two methods were chosen:

(a) Dialysis assay: dialysis tube (molecular weight cut o_, MWCO, 12–14000 Daltons, Visking Dialysis Membrane—Medicell Membranes Ltd., London, UK) was pre-activated, filled by 1 mL of NLC dispersion, and submerged in 350 mL of distilled water, keeping it protected from the light at room temperature and under gentle magnetic stirring. After 24 h,

both the dispersion inside the tube and the external aqueous phase were analyzed by UV-Vis analysis.

(b) Ultrafiltration assay: 0.45 mL of fresh NLC dispersion were placed in the upper chamber of a centrifugal filter tube (Ultrafree-MC, Millipore, cut-o_ 10,000 NMWL, and 30,000 NMWL) and then centrifuged (Microfuge 22R, Beckman coulter., Brea, CA, USA) at 8000 rpm at 4°C for 30 min. The aqueous solution collected at the bottom of the tube was subjected to UV-Vis analysis to determine the free CUR content[89].

2.15 Preparation of Sponges Loaded with Metronidazole and Curcumin Nanostructured Lipid Carriers

Two gels differing in composition were prepared:

- HyNa 2.50 g, PVP-K90 0.40 g, and TRH 15.0 g in 100 mL of water
- HyNa 4.0 g, PVP-K90 0.60 g, and TRH 10.0 g in 100 mL of water

An aliquot of 2 or 4 g of gel was added to the M7-300-TP or the M7-300-TP-MTR fresh dispersion, and the whole mixture was ultrasonically homogenized for 10 min with cycles of 0.7 s of activity and 0.3 s of inactivity by placing the container in an ice bath. The sample was frozen at -80°C for 24 h, and then moved to the freeze-drier (Labconco FreeZone® Kansas City, MO, USA 2.5 Liter Freeze Dry System), setting the vacuum at 0.014 mPa and -54°C of temperature and maintaining these conditions for 48 h. Sponge-C-MTR was the sample chosen for the next characterizations.

2.16 Porosity

The freeze-drying process allows removing the solvent from the formulation to obtain a porous structure, with air in the space previously occupied by the solvent. The sponge porosity, meant as total pore volume, was calculated mathematically according the following equation (5) [90]:

$$\%Porosity = \frac{practical\ volume - theoretical\ volume}{pratical\ volume} \times 100 \qquad (5)$$

As theoretical volume was considered the bulk volume of the total ingredients of one sample and was calculated according to the equation (6):

$$Theoretical\ volume = \sum \frac{m_n}{\rho_n} \qquad (6)$$

Where m and ρ are respectively mass and density of each ingredient.

The practical volume of sponge was determined placing the sample in a graduated cylinder and measuring the occupied volume (length x width x height)

2.17 Hygroscopic Measurement of Sponges

The ability of sponges to attract water molecules from the atmospheric moisture at room temperature was evaluated using an analytical balance (mod. AE 240, Mettler-Toledo S.p.A., Milan, Italy). Before each test, a desiccant box containing silica, was kept in the weighing chamber for 15 min.

Immediately after exiting the freeze dryer, an aliquot of sponge was weighed, and after the two side doors of balance were opened, allowing the sponge to contact the environmental moisture. At intervals of 10 min, the weight of the sponge was recorded prolonging the experiment until the powder showed no increase in weight. The increase in weight of each sample was calculated as follows (7):

$$\textbf{Weight increase } \% = \frac{W_t - W_i}{W_i} \, x \, 100 \qquad (7)$$

where W_t is the weight of sponge at time t, and W_i is the weight of dry sponge.

2.18 Quantitative Determination of CUR and MTR in the Sponges

A total of 5 mg of the lyophilized sponge was placed in a 20 mL flask, brought to volume with methanol, and sonicated until complete dissolution. Then, 1 mL aliquots were centrifuged (15,000 rpm for 2 min), and the supernatant was spectrophotometrically analyzed. The analysis was carried out on three aliquots from each lyophilized sponge.

2.19 Preparation of Minitablets

To standardize the sponge amount for the next analyses, minitablets were produced by compressing a precisely weighed amount (30 mg) of Sponge-C-MTR. A graduated mould having 5 mm diameter as well as a mobile upper and a lower plunger was used, obtaining a minitablet with a volume of 0.76 cm^3.

2.20 Swelling Test

Weight and optic assessments were used to perform the swelling tests on the minitablets.

The weight tests were carried out, weighting the minitablets by an analytical balance (Mettler, Columbus, OH, USA, Mod. AE 240). 0.5 mL of artificial saliva (pH 6.8) were added on the tables very 5 min for 20 min. At each timepoint, the excess water was removed with a filter

paper, and the weight was assessed. Tests were performed on six different minitablets, and results were reckoned following the Equation (8).

$$\textbf{Swelling Index} = \frac{\mathbf{W_0} + (\mathbf{W_t} - \mathbf{W_0})}{\boldsymbol{W_0}} = \frac{\boldsymbol{W_t}}{\boldsymbol{W_0}} \qquad (\mathbf{8})$$

where W_t is the weight of the minitablets at time t, and W_0 is the weight of the dry sample.

The optical assays were performed with both the plan and the frontal assessments. Samples were previously placed on a microscope slide and then on graph paper. Every 5 min for 2 h, 0.5 mL of simulated saliva (pH 6.8, 37°C) were added, and photographs were taken to evaluate any change on the minitablets' morphology.

2.21 Ex Vivo Permeation/Penetration Studies of CUR and MTR from Minitablets through L-PRF Membrane

The L-PRF membranes were prepared following the IntraLock protocol, previously described, and approved by the Food and Drug Administration (FDA).

The L-PRF membranes were fixed between the two compartments of the jacketed Franz type diffusion cells to perform the ex vivo permeation/penetration studies of CUR and MTR from minitablets. The donor chamber was filled by the minitablet and 0.5 mL of citrate buffer pH 6.2, while the citrate buffer pH 6.2 plus 4% (w/v) of Tween 20 was used as receiver fluids. The experiments were carried out on 3 h, withdrawing 0.5 mL every 5 min, replacing the same volume with fresh fluid, and keeping the system temperature at 37 ± 0.5 °C. At the end of each experiment, the amounts of CUR and MTR entrapped inside the L-PRF membrane were quantified by the extraction in methanol (3× 3 mL). The extracted liquors were collected, transferred in a 10 mL flask, and brought to volume with methanol.

2.22 MTT Cell Viability Assay

Homo sapiens bone marrow stromal cells (HS5) were grown in DMEM (ATCC® 30-2002) added with 10% fetal bovine serum (FBS) and antibiotics and maintained in culture in a humidified incubator under 5% CO_2 and 95% air at 37 °C. HS5 cells were seeded at 30.000 cells/cm^2 and, the day after, the medium was removed and substituted with fresh medium containing different concentrations of the empty nanocomposite sponge (without CUR and MTR), or Sponge-C-MTR. The following concentrations were tested: 0.025 mg/mL, 0.0502

mg/mL, 0.080 mg/mL, 0.12 mg/mL and 0.15mg/mL. MTT assay (Invitrogen M6494) was used to evaluate cell viability at 24 hours after the treatment.

2.23 Drugs Quantification by UV-Vis Methods

The amounts of CUR and MTR entrapped in the NLC suspension, the sponges, and the membranes were measured spectrophotometrically (UV-Vis mod. Pharma Spec 1700, Shimadzu, Tokyo, Japan) using the appropriate calibration curve and blank. The linearity was statistically determined by regression analysis of five concentrations in the range below specified and evaluated in triplicate. UV-Vis methods were found as simple, accurate, and reproducible.

For CUR determination, two calibration curves in methanol were performed at λmax = 428 nm: in the linearity range of 0.0002-0.0075 mg/mL, regression equation was Abs = -0.0289 + 132 x [mg/mL] (R = 0.999, SE 0.0101) and in the linearity range of 0.0025-0.01 mg/mL, regression equation was Abs = -0.0108 + 136 x [mg/mL] (R = 0.997, SE 0.0397).

For the calibration curve in phosphate buffer pH 6.2 plus tween 20 (4% w/v) in the linearity range of 0.0001-0.001 mg/mL, the regression equation was Abs = 0.01277+160 x [mg/mL] (R = 0.997, SE 0.0105).

For MTR determination were found validation parameters in methanol, in PBS and in Phosphate buffer pH 6.2 plus tween 20 (8% w/v), at λmax = 310 nm. For PBS, linearity range was 0.0025–0.0125 mg/mL, regression equation Abs = 0.0011 + 61.78 x [mg/mL] (R = 0.999, SE 0.0040). For Phosphate buffer pH 6.2 plus tween 20 (8% w/v), linearity range was 0.0025–0.02 mg/mL, regression equation Abs = 0.0771+ 46.8 x [mg/mL] (R = 0.998, SE 0.0102). Finally, for methanol, linearity range was 0.0025–0.03 mg/mL and regression equation Abs = 0.0011+ 62 x [mg/mL] (R = 0.999, SE 0.0092).

2.24 Data Analysis

Data were expressed as mean ± SE of at least three replicates (n = 3). For the statistical analysis of data, Student's t-test was applied with the minimum levels of significance with $p < 0.05$.

CHAPTER 3

Results

a) Leucocytes and Platelet rich Fibrin(L-PRF) for Guided Bone Regeneration and Alveolar Ridge Preservation

Fifth-teen patients aged between 29 and 70 (mean 49.4) years, including 9 females and 6 males completed the study. Each patient had tooth extractions, treatment of post extraction socket with L-PRF alone or in combination with PRF-Block and implant placement as rehabilitation approach.

3.1 GBR treatment

Five patients presented horizontal and/or vertical bone defects, mostly due to periapical cysts, thus GBRs were performed to augment the bone volume. Results and further information are shown in table 3.

Table 3: Results of GBR Treatments

PATIENTS	***1***	***2***	***3***	***4***	***5***
AGE	33	45	55	51	45
GENDER	M	F	M	F	F
TEETH RELATED TO THE BONE DEFECT	4.6-4.8	2.4	1.5-1.7	3.3-.34	1.4-1.6
GRAFT	L-PRF and PRF-Block	L-PRF and PRF-Block	L-PRF and PRF-Block	L-PRF and PRF-Block	L-PRF and PRF-Block
SMOKER	No	No	Heavy	No	No
SOFT TISSUE HEALING INDEX AFTER 7-10 DAYS	4	3	3	2	3
BONE REGENERATION AFTER 6 MONTHS	Yes	Yes	Yes	Yes	Yes

IMPLANT PLACEMENT	Yes	Yes	Yes	Yes	Yes

Radiological and clinical examinations after the treatment showed the integration of the grafts with the surrounding bone.

All patients showed uneventful postoperative wound healing, without adverse events. After 6 months from the GBR treatments, all patients showed evident bone regeneration and adequate bone volume for implant placement. Three months after implant insertion, radiographic evaluations showed a suitable osteointegration achieved in all the placed implants.

Patient 5 presented a lesion that led to critical-size defect formation. The GBR treatment performed on this lesion is reported as case report 1.

3.2 ARP Treatment

Ten patients were treated to prevent the resorption of alveolar ridges; five of them needed the exodontia due to the severe mobility of interested teeth ascribable to periodontal disease, while the others presented small cysts close to tooth roots. Results and further information are shown in table 4.

Table 4 Results of ARP Treatments

PATIENTS	***1***	***2***	***3***	***4***	***5***	***6***	***7***	***8***	***9***	***10***
AGE	45	55	70	55	48	38	59	68	29	45
GENDER	M	M	F	F	F	F	M	M	F	F
EXTRACTED TOOTH	1.4	4.6	1.6	4.5-4.6	1.1	4.5-4.6	3.1-3.3	4.7-3.6	4.5-.4.6	3.5-3.7
GRAFT	L-PRF	L-PRF	L-PRF	L-PRF	L-PRF	L-PRF and PRF-Block	L-PRF and PRF-Block	L-PRF and PRF-Block	L-PRF and PRF-Block	L-PRF and PRF-Block
SMOKER	No	No	Yes	No	No	No	No	No	No	No

SOFT TISSUE HEALING INDEX AFTER 7-10 DAYS	3	3	3	4	4	5	3	3	4	4
MAINTENANCE OF ALVEOLAR RIDGE DIMENSIONS AFTER 3 MONTHS	Yes	Yes	Yes	Yes	Yes	Yes	Yes	Yes	Yes	Yes
IMPLANT PLACEMENT	Yes	Yes	Yes	Yes	Yes	Yes	Yes	Yes	Yes	Yes

Radiological and clinical examinations after the treatment showed the integration of the grafts with the surrounding bone.

All patients showed uneventful postoperative wound healing, without adverse events. After 3-4 months from the ARP treatments, all patients showed slight and irrelevant changes in alveolar ridge dimensions, providing adequate bone volume for implant placement. Three months after implant placement, radiographic evaluations showed a suitable osteointegration achieved in all the placed implants.

Patient 5 underwent extraction due to the fractur of the anterior tooth; the ARP treatment performed on this extraction socket is reported as case report 2.

3.3 Case reports

3.3.1 Case 1– Guided bone regeneration of a critical-size alveolar bone defect

A non-smoker 45-years old woman complained a right-side facial pain and swelling, begun some days before the first clinical examination, that revealed abnormal mobility of teeth #14-16, previously endodontically treated, and pain response to percussion testing. There was no significant systemic complaint. The family history was unremarkable.

The dental radiographs showed the presence of a large cystic lesion referred to the mentioned teeth (Figure 9a). Thus, a CBCT with a multiplanar reconstruction program (MPR) was assessed to evaluate the three-dimensions of the lesion, showing a periapical lesion approximately 20 mm x 15mm x 14mm, with a soft, fluctuant, and cystic consistency,

resulting in a critical-size alveolar bone defect (Figure 9b, c, d). The final diagnosis was odontogenic cyst and teeth #14-16 with hopeless prognosis. Based on the findings, teeth extraction, cyst removal and GBR procedures combined with L-PRF and L-PRF block were planned (Figure 10).

Before the beginning of the surgical procedures, L-PRF and PRF block were prepared according to the techniques described in Material and Method section, as well as GBR surgery was performed following the protocol exposed in material and method section.

Histological examination confirmed the odontogenic nature of the cyst (i.e., periapical/radicular cyst) and in the following weeks, the patient was under strict oral hygiene measures and on regular recall. Soft tissue healing was uneventfully, no infection or swelling after the surgery. Bone tissue healing was observed with dental radiograph six months postoperatively (Figure 11a, b).

The second stage surgery, implant placement, was then performed and before the procedure an alveolar bone sample was obtained from the #15 implant site using a trephine bur (Figure 11c.). Three implants (Blossom, Intra-lock, USA) were placed in the area of teeth #14-16 (Figure 11d, e, f). The sample was processed and bone histomorphometry was performed (Figure 11g). Sutures were removed after 10 days.

Three months after implant placement, an impression was made; implants were loaded with screw-retained temporary fixed partial restorations. Definitive restoration was placed after 2 months (Figure 12a). The regeneration of bone tissue was highlighted with a new CBCT (Figure 11b, c, d).

The histological analysis showed that the L-PRF block was able to produce mature alveolar bone tissue, achieving the bone healing in about six months. The regenerated bone structure allowed the subsequent implant prosthetic rehabilitation; two months after their placements, the radiograph showed an adequate osteointegration of the implants in the novel bone.

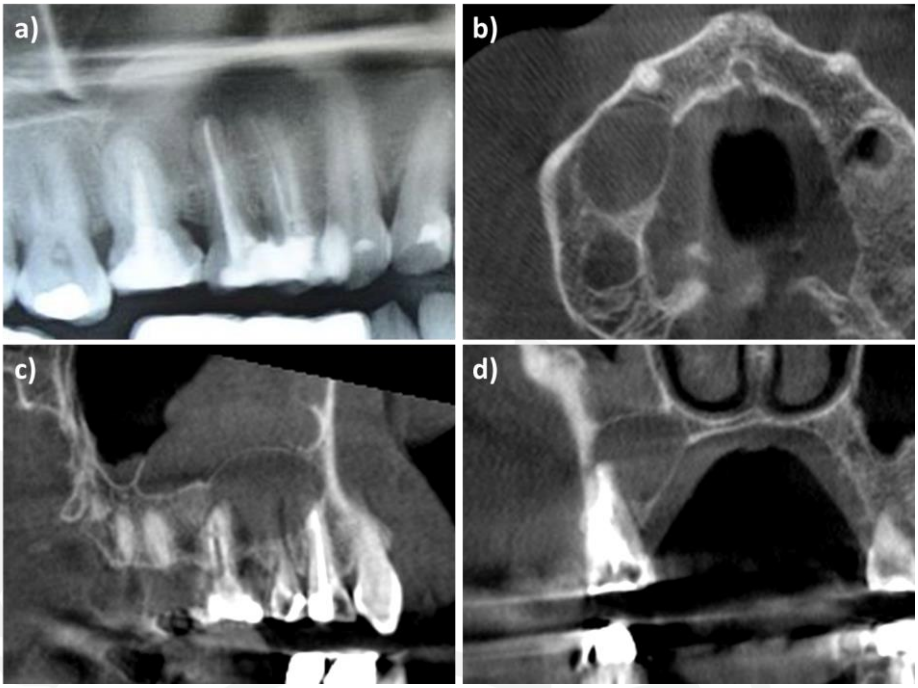

Figure 9: radiological examinations. a) detail of the dental radiograph at the first clinical examination; b) c) d) 3D CBCT scan before surgery.

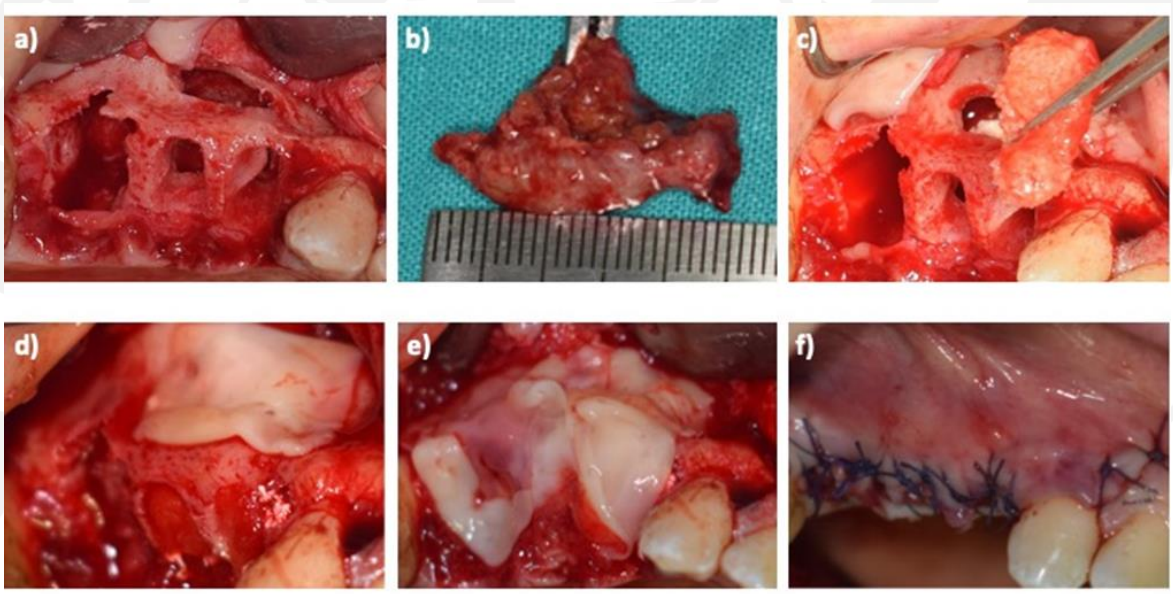

Figure 10: a) bone defect after dental extractions and cyst removal; b) cystic lesion; c) application of L-PRF clot under the sinus floor and L-PRF block in the bone lesion and post-extraction sockets; d) e) application of the remaining L-PRF clots over the surgical site; f) sutures.

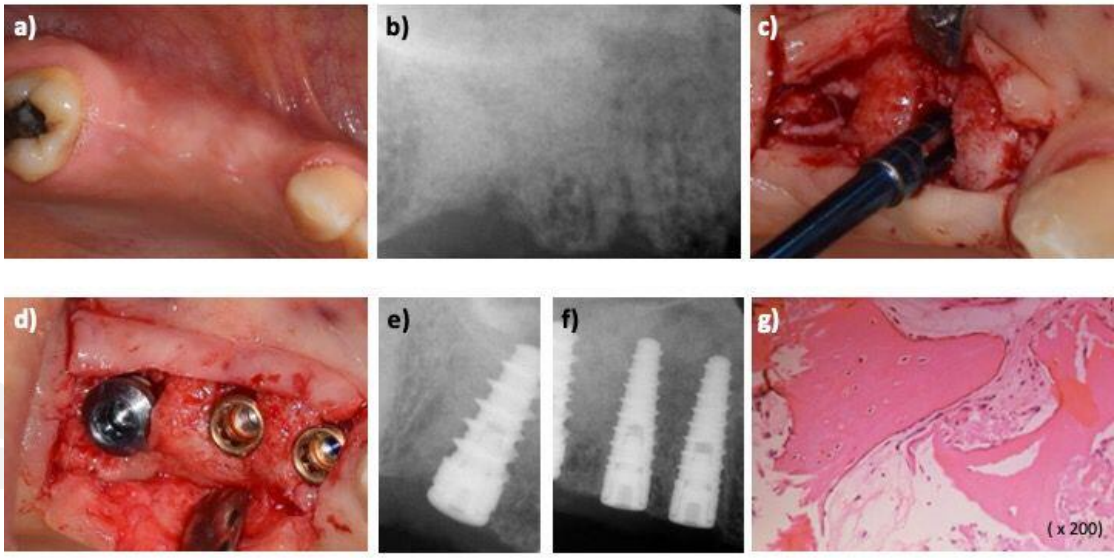

Figure 11: a) b) Six months post-surgical regeneration procedures, clinical and radiological view; c) bone sample harvesting procedure at the #15 implant site using a trephine bur; d) dental implants placement; e) f) intraoral radiograph after placing dental implants; g) magnification of histological findings of the bone sample (osteoblastic cells on the surface of the new woven bone containing osteocytes.

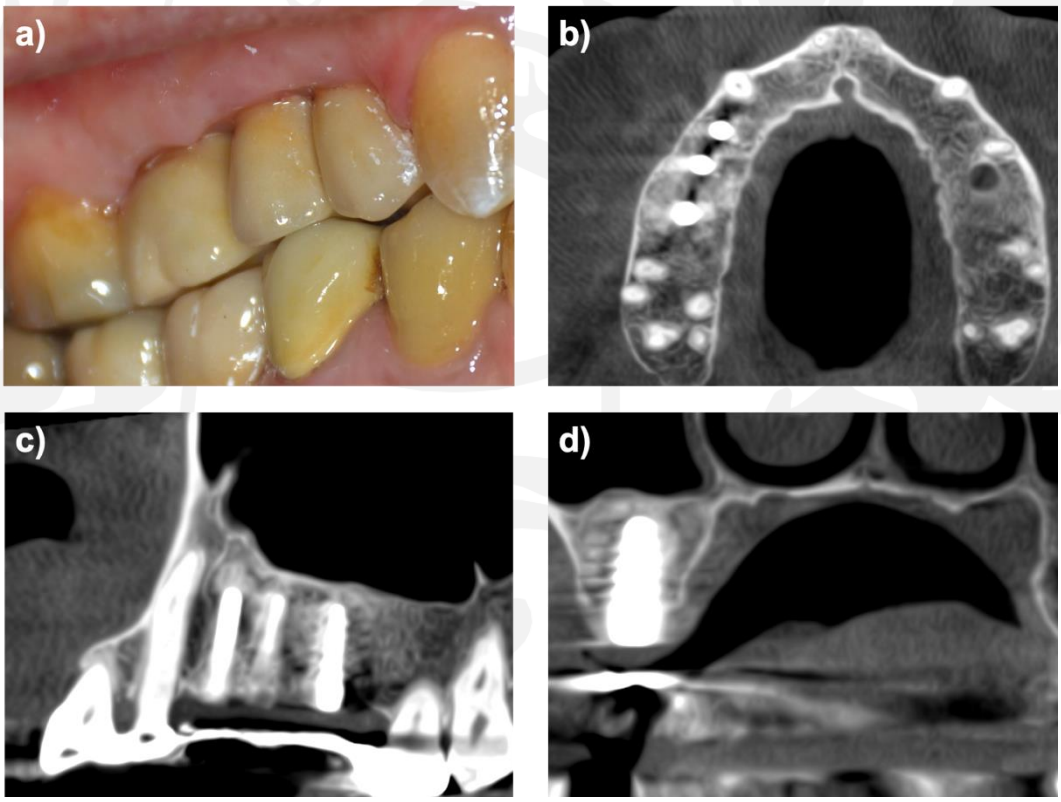

Figure 12: a) clinical view of the implant-based rehabilitation; b) c) d) 3D CBCT scan after implant placements.

3.3.2 Case 2 –Alveolar Ridge Preservation in a post extraction socket

A non-smoker 48-years-old female presented to our attention with a suspected fracture of the upper right central incisor (Figure 13a, b, c, d). Anamnestically, the patient reported no health concern and no consumption of tobacco or alcohol, and the family history was unremarkable.

The patient presented an orthodontic splint of upper anterior teeth, placed by a colleague to avoid tooth crown loss. Radiological examination confirmed the tooth fracture of the #11.

The severe mobility of the anchored fragment and root led to its extraction (Figure 13e) followed by the ARP procedure to prevent the ridge remodeling and alveolar bone resorption. L-PRF clots were applied, until the post extractive socket was completely filled (Figure 13f, g) and sutured to be stabilized (Figure 13h). The tooth crown was adapted on the previous orthodontic splint. Post-surgical antiseptic therapy has been prescribed to the patient. During the following weeks, the patient was under strict oral hygiene measures and on regular recall and soft tissue healing was achieved uneventfully.

After 3 months, the patient performed a Computed tomography (CT) dental scan. The clinical-radiological evaluations showed the presence of adequate and ample bone ridge (Figure 14a, b); thus, the implant placement was planned and performed (Figure 14c) and later the implant was successfully loaded.

At the latest follow-up, the clinical examination showed a good pink and white esthetics (Figure 14d).

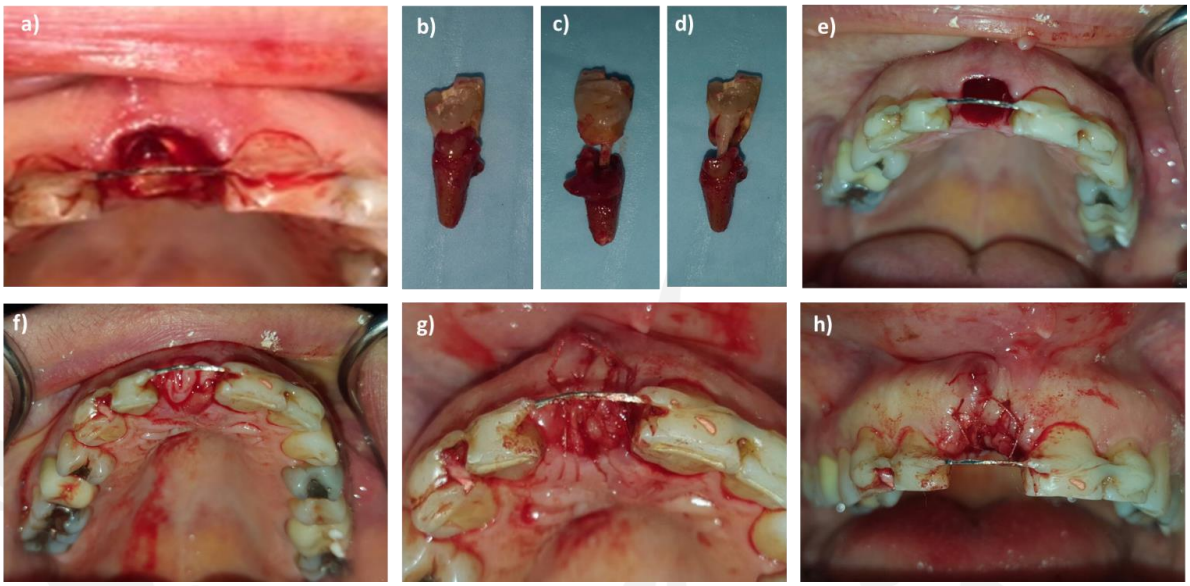

Figure 13: a) fracture of the upper right central incisor; b) c) d) root and crown fragments; e) post-extraction socket; f) g) application of L-PRF clots filling the alveolus; h) sutures.

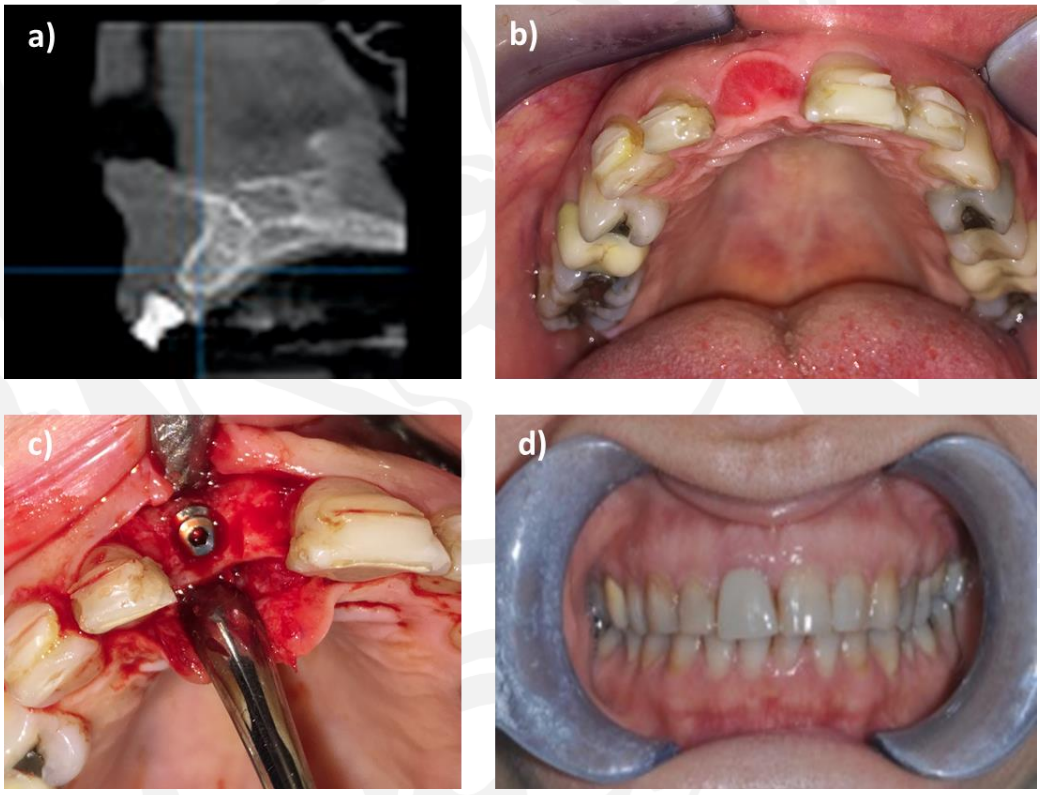

Figure 14: surgical site after three months: a) CT scan; b) clinical view; c) implant placement; d) last clinical examination.

3.4 Lipid ratio mixtures screening studies

The screening results obtained by visual inspection upon heating showed that none of the lipid mixtures in the tested ratios were able to solubilize CUR in an amount corresponding to 8% (w/w) of the whole mix. On the contrary, 5% CUR was completely solubilized when GA was present at 3%, and HEXA and IP were in 60:40 ratio (Table 5). The melting point of the MIX7 resulted in 48 ± 2 °C.

Table 5: Composition of lipid mixtures.

SAMPLE	*CUR (g)*	*GA (g)*	*HEXA (g)*	*IP (g)*	*HEXA: IP*	*Appearance*
MIX 1	0.08	0.10	0.49	0.33	60:40	Opalescent
MIX 2	0.08	0.10	0.41	0.41	50:50	Opalescent
MIX 3	0.05	0.10	0.51	0.34	60:40	Opalescent
MIX4	0.05	0.10	0.425	0.425	50:50	Opalescent
MIX 5	0.08	0.03	0.53	0.36	60:40	Opalescent
MIX 6	0.08	0.03	0.445	0.445	50:50	Opalescent
MIX 7	0.05	0.03	0.55	0.37	60:40	Clear

CUR: curcumin; GA: glycyrrhetic acid; HEXA: 1-hexadecanol; IP: isopropyl palmitate

3.5 Preparation of CUR-Loaded NLC Dispersion Enriched in Metronidazole

MIX7 was chosen to prepare the CUR loaded NLCs, that were obtained by homogenization followed by probe sonication method. To avoid the pH-dependent CUR decomposition[91], the pH 6.2 citrate buffer was chosen as aqueous medium. All the NLC dispersions obtained by changing both the lipid mixture ratios and the surfactants (Table 6) were homogeneous, stable, and easy to re-disperse.

Table 6: Composition of prepared NLCs using 20 mL of aqueous medium.

SAMPLE	*AMOUNT OF MIX7 (mg)*	*TW80 (mg)*	*F-68 (mg)*
M7-100-T	100	200	-
M7-200-T	200	200	-
M7-300-T	300	200	-
M7-100-TP	100	200	200
M7-200-TP	200	200	200
M7-300-TP	300	200	200

3.6 Characterization of Nanostructured Lipid Carriers

3.6.1 Particle Size, Polydispersity Index, and Zeta Potential Analysis

DLS measurements of nanoparticle mean particle size (Z-average), particle size distribution (PDI), and electrical charge (Z-potential, ζ) were performed to investigate the stability of the NLC dispersions and choose the one with the best parameters. Table 7 shows Z-average, PDI, and Z-potential values of all the studied formulations. According to these results, M7-300-TP was chosen to prepare subsequent formulations.

Table 7: Mean particle size (Z-average), particle size distribution (PDI), and electrical charge surface (ZP) of NLC formulations. Values are expressed as mean ± SD (n = 3).

Samples	***Z-Average (nm)***	***PDI***	***Z-Potential (mV)***
M7-100-T	121.8± 15.44	0.372	−20.5 ± 6.8
M7-100-TP	117.9 ± 32.81	0.290	−19.5 ± 5.1
M7-200-T	88.5 ± 8.68	0.733	−19.5 ± 6.44
M7-200-TP	182.2 ± 36.88	0.265	−13.5 ± 7.95
M7-300-T	689.4 ± 17.08	0.709	−20.5 ± 5.87
M7-300-TP	157.0 ± 25.52	0.403	−25.5 ± 7.79
M7-300-TP-MTR	112.0 ± 28.56	0.337	−24.0 ± 5.32

3.6.2 Morphology by Scanning Electron Microscopy (SEM) and Transmission Electron Microscopy (TEM)

To confirm NLCs shape and size as well as to investigate their surface morphology, the electron microscopy scan (SEM) was performed on M7-300-TP-MTR, and the micrographs are shown in Figure 15a. The nanoparticles appeared with spherical and smooth shapes, and the sizes were less than 200 nm; moreover, no crystalline structures of MTR were observed.

In Figure 15b are reported TEM images of single NLCs loaded only with CUR and CUR-MTR. As can be noticed, the detail of the single NLCs shows an average size of 50 ± 10 nm and well-defined circular structure.

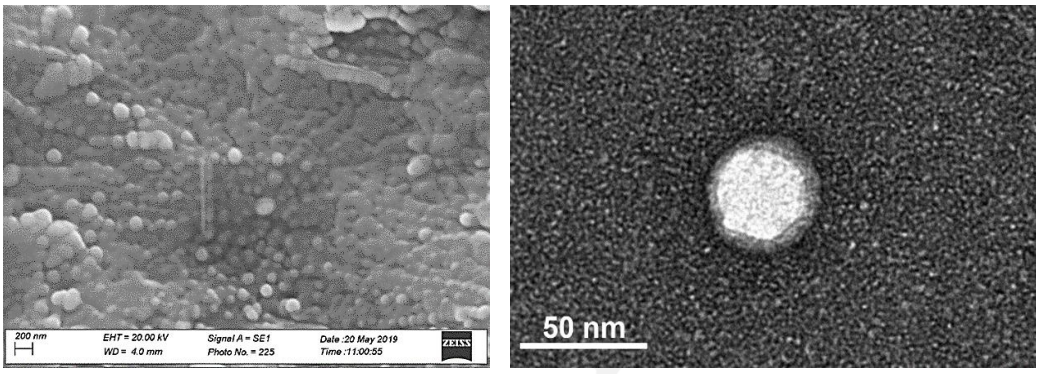

(a) (b)

Figure 15: SEM morphology of dried dispersion M7-300-TP-MTR; bar = 200 nm. (b): TEM image of single NLC from M7-300-TP-MTR batch; bar = 50 nm.

3.6.3 Entrapment Efficacy (EE) of NLC

Preliminarily, the amount of CUR and MTR in the fresh NLC dispersion, expressed in terms of DR, was determined to evaluate the amount of active and inactive ingredients lost during the preparation step. CUR and MTR recovery (DR) was calculated using the effective volume of the fresh NLCs dispersion recovered, resulting in 93 ± 1.63% and 88 ± 2.04% (mean ± SE), respectively. Entrapment efficacy (EE%) and loading capacity (LC%) of NLCs were indirectly determined by quantification of the free CUR in the aqueous phase (unentrapped) by both dialysis and ultrafiltration methods. Since no free CUR was detected by both the analyses, the EE and the LC resulted respectively in 100% and 5% of recovered materials.

3.7 Sponges Loaded with MTR and CUR-NLCs Formulation and Characterization

Different samples were obtained changing the amount of gel used and they are reported in Table 8.

All the samples appeared solid, friable, and uniform in color after drying, but an alteration of Sponge-A and Sponge-A-MTR occurred once in contact with the environmental temperature and moisture. In fact, when they were taken out of the freeze dryer, they became brown and sticky, also showing hygroscopicity.

Table 8: Nanocomposite sponge compositions.

	COMPOSITION OF EACH BATCH OF COMPOSITE SPONGES (MG)							
	CUR-NLC	***MTR***	***HyNa***	***PVP-K90***	***TRH***	***Tw80***	***P-68***	***Buffer Salts***
SPONGE-A	M7-300-TP	0	50	8	300	200	200	57
SPONGE-A-MTR	M7-300-TP-MTR	150	50	8	300	200	200	57
SPONGE-B	M7-300-TP	0	100	16	600	200	200	57
SPONGE-B-MTR	M7-300-TP-MTR	150	100	16	600	200	200	57
SPONGE-C	M7-300-TP	0	160	24	400	200	200	57
SPONGE-C-MTR	M7-300-TP-MTR	150	160	24	400	200	200	57

The ability of the sponges to take up moisture from their surroundings were evaluated as weight increase over time. The solid-state of the samples was ensured during the experiment, to exclude potential transformations once the moisture was absorbed. In Figure 16 was reported the gradual increase of the weight up to 30 min. At this time, a plateau was observed, suggesting that the equilibrium with environmental moisture was reached. Based on these results, the less hygroscopic sponges were chosen for next characterizations.

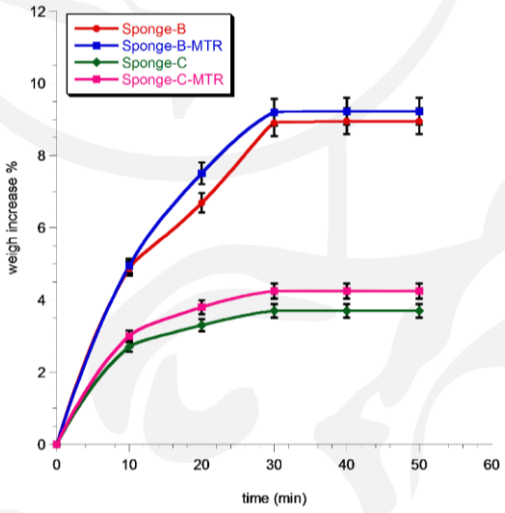

Figure 16: Percent of weight increase of sponges maintained in environmental moisture over time. Data represent mean ± SE (n = 3).

The amount of the active compounds was evaluated by analyzing different portions of powder of the same batch and quantifying the drugs by UV-Vis analysis. CUR and MTR resulted in 0.9 ± 0.03% and 9.5 ± 0.02% w/w, respectively, showing a homogeneous distribution of active compounds in the whole samples.

The structure and the morphology of sponges were investigated, as well as the porosity of Sponge-C and Sponge-C-MTR, that resulted in 93.15 ± 0.14% and 92.86 ± 0.18%, respectively.

The porous nature of Sponge-C-MTR was confirmed by SEM images (Figure 17). The porous structure was plainly visible, with pores having an average diameter of about 10–20 µm. However, higher resolving power of SEM damaged the sample, thus the presence of NLC trapped in the matrix could not be investigated.

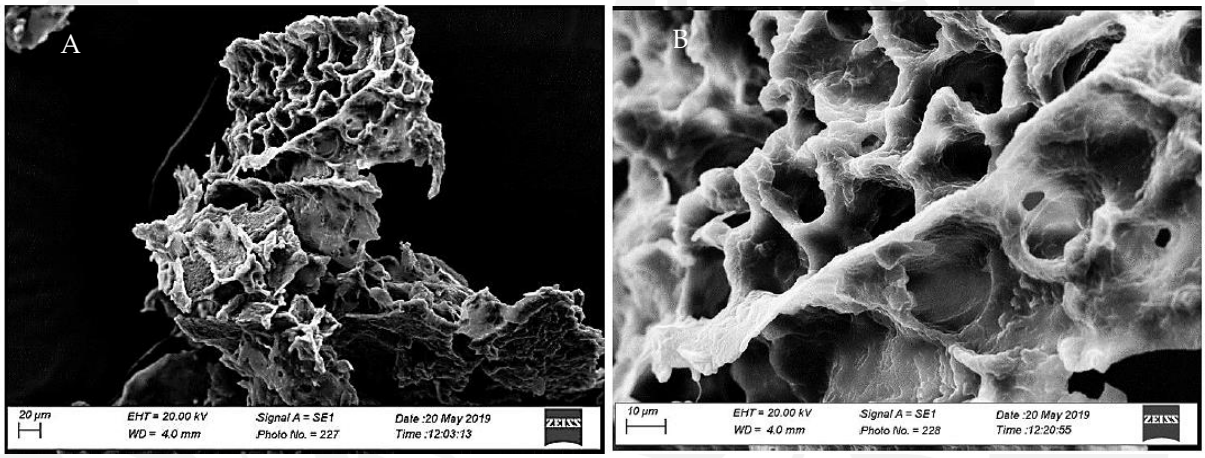

Figure 17: SEM images of surface morphology and internal structure of Sponge-C-MTR. (A) magnitude bar = 20 µm; (B) magnitude bar = 10 µm.

3.8 Preparation of Minitablets

Afterwards, minitablets were obtained by compacting definite amounts of Sponge-C-MTR until a definite volume (Figure 18). Average tablet weight, diameter, and thickness resulted in 30 ± 1.2 mg, 4.5 ± 0.05 mm, and 2.5 ± 0.05 mm, respectively.

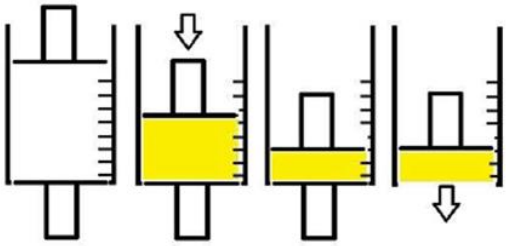

Figure 18: Schematic representation of the process to obtain the minitablets.

3.9 Swelling Test

The maximum swelling degree was reached after 15 min, corresponding to a 2.7-fold increase of the initial weight, due to saliva absorption by minitablet forming a viscous gel layer around it. Figure 19 shows minitablet weight variations expressed as the increase in the initial weight versus time.

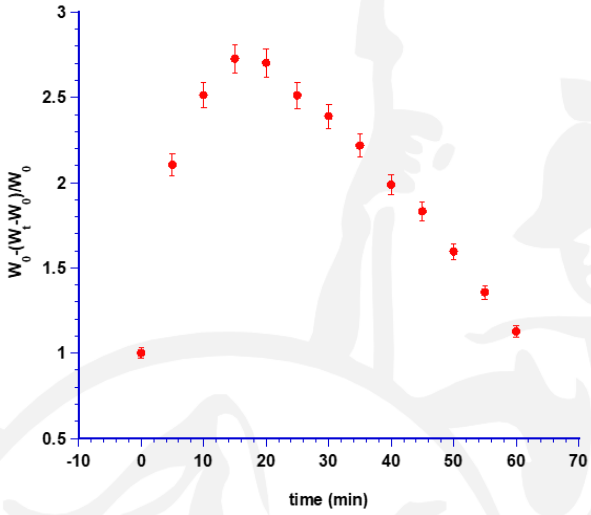

Figure 19: Swelling index measured as weight increase versus time. Data are presented as means ± SE.

The swelling aptitude of the minitablets was also evaluated by frontal and radial visual assessments (Figure 20). In both assessments, a partial loss of weight and dissolution occurred in 120 min.

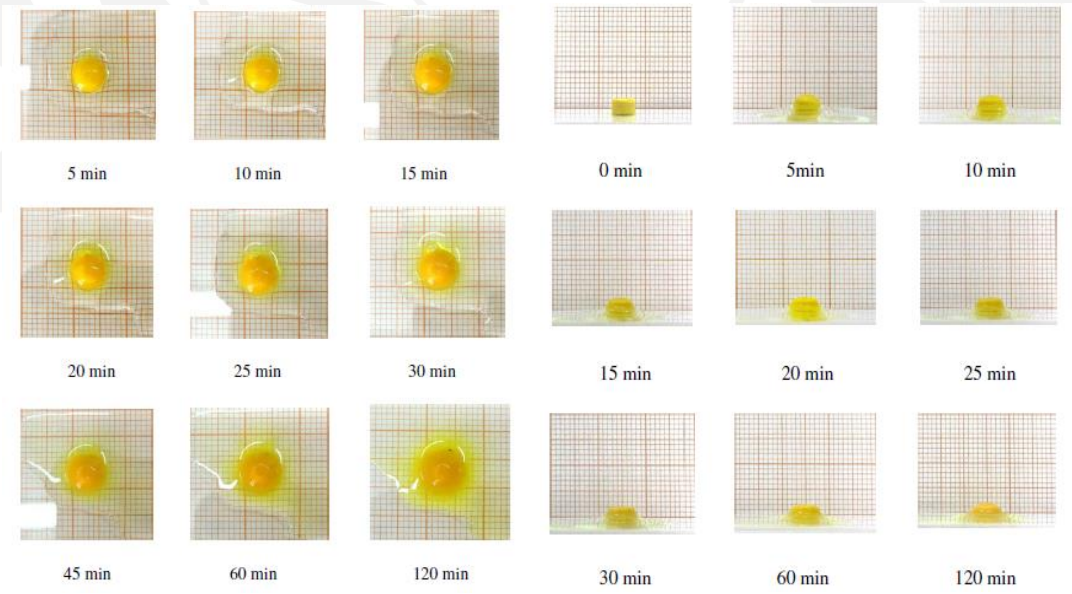

Figure 20: Timeline from 0 to 120 min of radial and frontal swelling of the minitablet.

3.10 Ex Vivo Permeation/Penetration Studies of CUR and MTR from Minitablets through L-PRF Membrane

The ability of the minitablet to promote CUR and MTR permeation rather than penetration in the L-PRF clot was evaluated mounting L-PRF clot as a membrane in Franz type diffusion cells and applying minitablet to the apical side.

No CUR was detected in the acceptor compartment, while the results of MTR amounts permeated in the acceptor chamber versus time are shown in Figure 21. The extrapolated flux (Js) per unit area of MTR through the L-PRF membrane resulted in 0.457 mg/cm^{2}h.

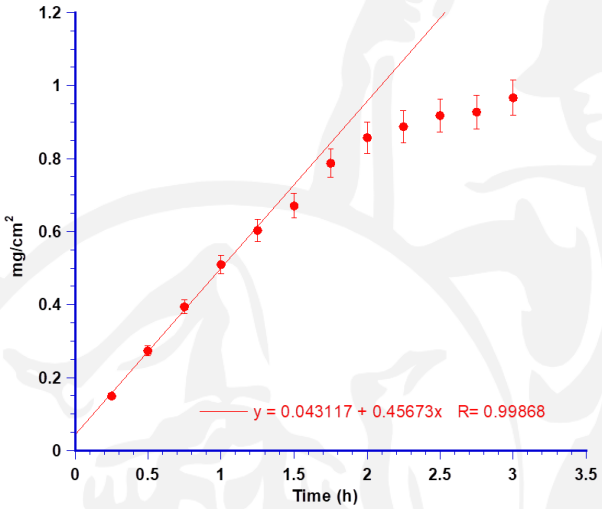

Figure 21: Permeation data of MTR per cm2 throughout the L-PRF membrane and linear fitting at the steady-state concentrations. Values are presented as means ± SE (n = 6).

The amounts of CUR and MTR accumulated in the L-PRF membrane at the end of each experiment (Figure 22) were evaluated by methanol extraction. The extracted CUR and MTR, expressed as a percent of the dose administered, resulted in 1.76% w/w and 2.5% w/w, respectively.

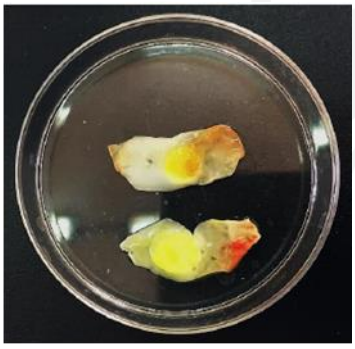

Figure 22: L-PRF membranes before after permeation tests.

3.11 MTT Cell Viability Assay

The MTT assay was performed after 24h incubation using a concentration range of 0.025-0.15 mg/ml. Cell viability was almost not affected by the Sponge-C-MTR, resulting in 80-90% referred to untreated control cells for the whole concentration range analyzed. On the other hand, the treatment with any concentration of the empty sponge led to viability between 80-70% respect to untreated control indicating a borderline cytocompatibility (Figure 23).

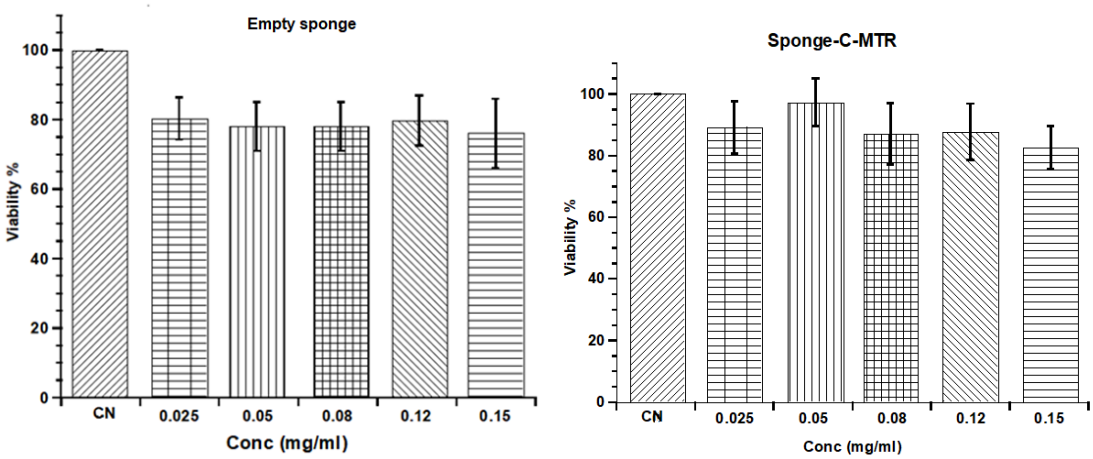

Figure 23: Cell viability of HS5 cells after 24h of treatment at different concentrations of the empty nanocomposite sponge or Sponge-C-MTR, compared to the cell viability of untreated cells (CN). Results are the means ± SE of three separate experiments.

CHAPTER 4

Discussion

a) Leucocytes and Platelet rich Fibrin(L-PRF) for Guided Bone Regeneration and Alveolar Ridge Preservation

The study aimed to evaluate the effect of L-PRF in its pure form and as L-PRF block in socket wound healing after tooth extraction as noticed by soft tissue healing, increased bone fill, and reduced alveolar bone width resorption allowing reliable implant prosthetic rehabilitation.

Exodontia is one of the most common oral surgery procedures, indispensable when no other endodontic or preservative treatments can be used. Though, patients could undergo post-operative discomfort and complications that could significantly affect the oral health-related quality of life. Hence, the achievement of a better-quality life for patients after the tooth extraction procedures is still a challenging goal for oral surgeries and researchers.

The lack of one or more dental elements is often restored by implant placement, allowing appreciable functional and aesthetic rehabilitation. However, the *conditio sine qua non* to achieve reliable and long-lasting outcomes is the presence of adequate bone volume and ridge dimensions in the placement site. Widely strategies have been developed to rehabilitate deficiencies in bone volume occurring after tooth extraction, due to the natural ridge dimension remodeling and alveolar bone resorption, or in case of bony lesions. In particular, different GBR and ARP techniques have been proposed to regenerate bone defects or prevent bone resorption. Among graft materials currently used in oral procedures, autologous bone blocks have been often described as the gold standard. However, despite the proven success of these substitutes, they present some shortcomings such as the need for a second oral surgical site that, especially if outside the oral cavity, is related to higher patient morbidity and discomfort which can adversely affect the clinical outcomes as well as the quality of life[92]. Differently, in the case of the allografts, the main issues are related to their quality control, that has a direct impact on the clinical outcomes since disease transmission and infection control is of high significance, due to the cadaverous nature of these grafts[93].

Anyway, the use of grafts for socket preservation increases the treatment cost as well as the risk of disease decline and since they could not be totally incorporated into the newly formed,

they tend to show limited vital bone formation[27]. These drawbacks lead to increase the attention of clinicians in the selection of the type of graft that minimizes the adverse effects. The application of Non-Transfusional Hemocomponents as graft substitutes in oral surgery has been proposed with heterogeneous results.

The use of platelet aggregates for the management of postoperative pain and discomfort, as well as the rapid healing of the soft and hard tissues of the post extraction socket, has been recently proposed as a reliable and popular alternative[55,57,94]. Besides, the role of L-PRF, the second-generation of platelets concentrated, in these processes has been lately investigated[95,96].

In the present study, the soft tissue recovery has been examined using the healing index system described by Landry et al. (1998)[97]. Once sutures were removed, after 7-10 days, comparable healing of the soft tissues was achieved both in GBR and ARP groups. These results are in accordance with a recent study by Mourão et al. in 2020[67], where better healing was observed in the sockets that received L-PRF when compared to the sockets with spontaneous healing, highlighting that the use of L-PRF should be considered whenever improved healing is required.

Different mechanisms can be associated with soft tissue rehabilitation procedures based on L-PRF application. The recruitment and stimulated proliferation of several cell types, including fibroblasts, and the promotion of collagen synthesis has been shown to be related to the released growth factors by in vitro studies[98,99]. The clotting activation, essential event to enhance the haemostasias, is favored by the cytokines found in L-PRF[67,100]. The formation of a fibrin matrix with a complex trimolecular structure that offers greater resistance, elasticity, and resembling a natural matrix is attributable to fibrinogen and thrombin, that are concentrated in this platelet aggregate. The stimulation of chemotaxis, angiogenesis, proliferation, differentiation, and modulation, especially in the early stages of healing, by the released growth factors and cytokines is plentifully supported.

The ability of L-PRF to reduce post-operative pain, swelling and enhance the soft tissue healing seems to be experimentally and clinically supported, while the action on bone tissue regeneration is still controversial.

In this study, the use of L-PRF alone or in combination with the PRF-Block for alveolar bone regeneration or preservation led to interesting results. In GBR group, adequate horizontal

ridge augmentations were achieved in all the patients affected by bony defects. In ARP group, the use of L-PRF as a filling material for socket preservation seemed promising in order to maintain an adequate volume of soft and hard tissues and obtain aesthetic rehabilitations.

In all cases, bone volumes allowed implant-based rehabilitation within six months and a suitable osteointegration, critical factor for the long-term success and stability of implants, was achieved in all the implants three months after their placement.

As regards the case report 1, to our knowledge, this was the first case regarding the application of L-PRF and L-PRF block for the management of large cystic removal and extraction of three teeth.

L-PRF played a key role in remineralization, already significant six-months after the application. Although one standard definition for a critical-sized defect is not available, alveolar bone defects measuring 2-3 cm in diameter usually heal in about 12 months[101,102]. In our case, the bone healing was achieved in about six months, moreover, our histological analysis showed that the L-PRF and PRF block were able to produce mature alveolar bone tissue. These results could be related to L-PRF strong architecture, composed of micropores and thin fibres that allows it to serve as a scaffold for osteogenesis cell migration, differentiation and neovascularization, keeping the slow release of growth factors, as mentioned above, up to a period of 7-14 or 21 days[54,61]. Moreover, the preservation of bone ridges and the enhancement of the newborn formation could also be attributable to PRF-Block, that might be considered as a biomaterial for tissue engineering[65], since formed by biocompatible bone graft material processed with L-PRF membranes and fixed with liquid fibrinogen. In PRF block, the L-PRF acts as a biological connector among the graft particles, creating a matrix with suitable manipulative qualities and rich in bioactive molecules and growth factors[54,64,103,104]. Indeed, if it is well-known that xenografts can support osteoblast attachment and proliferation, several in vitro studies concluded that these effects can be further enhanced when PDGF is on their surface, indicating that growth factors on/or near to the xenografts might influence osteogenesis in vivo[105,106].

The stimulation of chemotaxis, angiogenesis, proliferation, differentiation, and modulation, especially in the early stages of healing, by the released growth factors and cytokines, is plentifully supported. The release kinetics of growth factors and cytokines from L-PRF and PRF-block have been also investigated. According to Lourenco et al., 2018, these substances are highly expressed with the 24h from L-PRF membrane, leading to an initial release that

may improve the clot formation and stabilization in the socket and have a role in the enhancement of the healing process. Besides, after the pronounced release in the first 24h, the release of these substances from the L-PRF membrane continues for up to 21 days[100]. While, in a study presented by Castro et al., 2019, a continuous release of growth factors from both L-PRF membrane and Block have been verified up to 14 days, even though the amount of growth factors was not the same. Indeed, the L- PRF exudate and the Liquid Fibrinogen embedded in the Block seemed to act as bioactive agents, affecting the release of growth factors, especially for levels per time interval of VEGF and BMP-1, while the L-PRF membrane seems to produce a higher concentration of TGF-β1 and three times more PDGF-AB than the L-PRF block[65].

However, the interesting healing profile of PRF block has been only recently investigated and just few authors have reported its use in human oral surgeries (about 26 intervention on 15 cases)[59,103,107], even though promising results have been collected. In a single cohort observational study, Cortellini et al. performed 15 bone augmentation procedures on 10 patients (mean age 50.7 years) affected by horizontal bone defects. The surgical procedures were based on the application of L-PRF block (a combination of two L-PRF membranes, 0.5 g deproteinized bovine bone mineral and liquid fibrinogen), collagen membrane and L-PRF membranes. A significant horizontal ridge augmentation was achieved, allowing implant placement in all cases[103]. Chenchev et al. evaluated the possibility for augmentation of the alveolar ridge in the frontal region of the upper jaw in an 18-year-old male applying a combination of bone graft materials, injectable platelet-rich-fibrin (i-PRF) and advanced platelet-rich fibrin (A-PRF). This augmentation procedure was a successful and the dental implant was placed[107]. Andrade et al. published a pilot clinical study on four patients, they applied a “dentin block” (a mixture of particulate autologous dentin with chopped L-PRF membranes, and liquid fibrinogen) in ten extraction sockets. The “dentin block” was able to promote new bone formation, without host tissue reactions, and a favorable dentin resorption/bone formation rate. All patients demonstrated an adequate amount and quality of bone for implant placement[59].

Despite the limitations related to the use of an innovative procedure, the obtained positive outcomes in terms of bone healing and tissue regeneration were in accordance with the literature and reinforced the effective role of L-PRF and its derivates in oral surgical procedures.

b) Technological approach for tissue regeneration

CUR possesses extremely low aqueous solubility in both neutral and acidic pHs, with a reported value of 11 ng/mL in aqueous pH 5.0 buffer solution, while it is soluble in ethanol, methanol, and acetone[108]. Moreover, a rapid CUR decomposition in neutral-basic pH conditions is well known[109]. On the other hand, due to its poor solubility and high instability in aqueous fluids, CUR is an excellent candidate for the development of formulations using nanoparticle lipid systems[110].

In the pharmaceutical field, nano-encapsulation is highly exploited to promote the absorption of substances that, as such, would not cross biological membranes. Therefore, using natural and/or synthetic materials is possible to obtain formulations suitable also for CUR administration. The physicochemical characteristics of lipid materials, such as lipid miscibility, polymorphism, and stability, as well as the surfactant effect on structure and type of nanoparticles are the most relevant parameters to take into account in NLC formulation[111]. Moreover, among all the lipid materials, those that do not undergo light or heat degradation, or oxidation processes must be chosen. From the biological point of view, the excipients used for NLCs must be non-carcinogenic or teratogenic, non-allergenic, and removed from the body through the physiological metabolic processes. Since the biocompatibility of all the components with the biological tissues is necessary, and considering the lipid nature of the active ingredient, the choice fell on 1-Hexadecanol (HEXA), isopropyl palmitate (IP), and 18-β glycyrrhetic acid (GA).

HEXA is a long-chain fatty alcohol widely used in cosmetic products, possessing emollient properties and weak antimicrobial activity[112]. IP is a branched and low molecular weight liquid ester owing emollient characteristics, suitable solvent capacity for lipophilic active ingredients and easily absorbed. GA is an active triterpenoid metabolite of glycyrrhizin extracted from the dried roots and rhizomes of Glycyrrhiza glabra, existing as α and β stereo-isomeric forms[113]. This well-known compound shows beneficial effects as skin whitening and anti-inflammatory agents in acute and chronic dermatitis, reducing skin lesion sizes and antioxidant activity against b-carotene destruction and LDL) oxidation[114]. Furthermore, antiviral, antibacterial, antifungal, antitussive, anti-diabetic, anti-diuretic, anti-ulcer, antihepatotoxic, cytoprotective, and cytotoxic effects were also demonstrated[115–117].

To prepare NLCs with high CUR loading and adequate stability, the complete solubilization of CUR in the used lipid mixture is necessary. Therefore, it was essential to investigate CUR solubility in the lipophilic mixture by varying the ratio of lipid components, thus the solubility of CUR at 5 and 8% w/w of the whole mixture was tested, modifying, in turn, lipid components ratios.

NLC dispersions were prepared using one or the mix of two surfactants, as well as different amount of LM chosen. Nanoparticles mean particle size (Z-average), particle size distribution (PDI), and electrical charge (Z-potential, ζ) were analyzed to characterize the NLC dispersions and choose the one with the best parameters. In fact, DLS measurements provide the parameters usually investigated to value the colloidal system stability. Acceptable NLC dispersions have PDI values between 0.1–0.4, indicating that the lipid nanoparticles are monodispersed, with narrow population sizes, low variability, and no aggregation. Likewise, NLCs with Z-potential value close to -30 mV are considered stable because the electrostatic repulsion between particles with the same electrical charge prevents aggregation.

The combined use of Tween 80 and Pluronic F-68 as surfactants had a high influence on the results, especially on PDI values since less width of the particle size distribution was observed. Due to a synergic action between the two emulsifying agents, mixed films formed on nanoparticle interfaces, leading to better surface coverage and increased viscosity and enhancing the long term stability of the formulation[111,118]. According to these conditions, M7-300-TP showed the most suitable values for all the studied parameters and was chosen to prepare subsequent formulations.

Since the aim of the work was to obtain a bifunctional nanocomposite also loaded with the antibacterial agent MTR, its physicochemical characteristics were also considered. MTR shows high solubility in water (10.61 mg/mL), particularly at a low pH, having pKa (basic) of 2.49 and LogP = −0.02[119,120]. Therefore, it is conceivable that MTR could remain entrapped in the hydrophilic portion of the composite drug delivery system designed by us. However, its solubilization rate is low, and the risk of MTR not being wholly solubilized in the next step of sponge formation was high. Therefore, to be sure that the whole MTR dose (150 mg) was solubilized in the aqueous phase of the dispersion, MTR was added in the first step NLCs preparation, obtaining the sample M7-300-TP-MTR. The formulation was characterized and compared in terms of Z-average, PDI, and Z-potential to the others in order to evaluate MTR effects on these parameters. Both average particle size and PDI values decreased when MTR

was added to the formulation, while Z-potential values were not significantly affected by it. Thus, the M7-300-TP-MTR sample was further characterized.

The SEM analyses on shape, the size and surface morphology of M7-300-TP-MTR showed a homogeneous dimensional distribution. Plus, no crystalline structures of MTR were observed, suggesting the absence of drug crystals in the dispersions. Some particle agglomerations were detected, probably due to the sticky nature of lipids as well as the treatment performed on the sample prior to the SEM analysis.

CUR and MTR recovery (DR) were reckoned on fresh dispersion, while the entrapment efficacy (EE%) and loading capacity (LC%) of NLCs were indirectly determined by quantification of the free CUR in the aqueous phase (unentrapped) by both dialysis and ultrafiltration methods. The obtained results confirmed the high affinity of CUR towards lipid mixtures and optimal experimental conditions to produce NLCs. Regarding MTR, by the analyses, up to 94% of the drug was unentrapped, demonstrating that, during the NLCs synthesis, MTR remained in aqueous medium, and about 5% could be partitioned among the NLCs. However, this did not alter the NLCs characteristics.

As regards the sponges, they were obtained entrapping M7-300-TP or M7-300-TP-MTR dispersions in a bioerodible hydrophilic polymers matrix and freeze-drying the samples. The matrix should be capable of adhering to the post-extraction socket tissues and swell once soaked by the physiological fluids, allowing the release of the antibiotic and the NLCs containing the antioxidant agent. This formulation was designed following two aims: (1) to allow the tissue penetration of CUR, otherwise insoluble in biological fluids, by its conveying into lipid nanoparticles; (2) to promote MTR prolonged loco-regional release in the post-extractive socket to preserve aseptic conditions of the target. To achieve the latter purpose, suitable hydrophilic polymer matrices were formulated. A mixture of polymers, such as hyaluronic acid and PVP, was chosen to prepare a three-dimensional network to entrap NLC dispersion and obtain a solid composite such as a sponge by freeze-drying method. Hyaluronic acid (HA) was selected as biocompatible and biodegradable polymer, used in the dental field as wound healing and adjuvant in tissue regeneration[121]. Polyvinylpyrrolidone (PVP-K90) is one of the most utilized pharmaceutical polymers for its chemical and biological inertia. It has been shown to have an excellent affinity with mucins and a capability of forming solid matrix systems (e.g., films, tablets, discs) with enhanced mucoadhesive properties[122,123]. In addition, Trehalose (α-D-glucopyranosyl-α-D-glucopyranoside, TRH) a

hydrophilic and biocompatible sugar as a cryoprotective agent, was added. Due to the ability to establish hydrogen bonds with bio-structures, TRH is able to prevent the degradation of biological materials replacing water or interposing itself between water and them[124].

Sponge-A and Sponge-A-MTR were discarded for the excessive hygroscopicity, attributable to the too low amount of polymers, which did not allow the maintenance of separation among the lipid nanoparticles, leading to the mutual blending of them. On the other hand, the Sponge-C and Sponge-C-MTR resulted the least hygroscopic.

The obtained multicomposite systems were characterized by a porous structure shaped by the water removal during the freeze-drying process, thus generating the vacant spaces, which contributed to the recognized large number of pores. Porosity is the collective term for these pores and their distribution in the structure of the solid. This morphological characteristic influences the ability to adsorb biological fluids as well as release drugs and nutrients embedded in it. The fluid absorption would be cooperative in controlling asepsis at the post-extractive sockets[125] and porosity causes an improvement in cell gas exchange, epithelium regeneration, exudates removal, and hemostasis[126,127]. Of note, that scaffold porosity has been reported as being more than 90% for tissue engineering applications[128].

Minitablets were designed to give to the formulation suitable form and dimension for the post-extraction socket to standardize the drug administration dose and to be easily placed into the target size. The reproducibility of the preparation method was confirmed by the obtained average tablet weight, diameter, and thickness, and by assessing the data following the Italian Pharmacopoeia [F.U. XII ed.] requirements.

Swelling tests as weight and visual assessments were performed on to evaluate the morphological changes that may occur in the tablets once in contact with the post-extraction cavity fluids as well as water penetration and sponge hydration ability. The samples weight decreased after 15 min due to erosion phenomena of the gel layer and dissolution of MTR together with hydrophilic sponge components, that were removed together with the excess of artificial saliva during the experiment.

Also, the frontal and radial visual assessments, performed to exclude any discomfort due to the morphologic changes and to ensure good patient compliance, showed a low aptitude of the minitablets to swell.

Recently, non-transfusional hemocomponents have been more and more applied in several dental and oral surgeries procedures, such as the preservation of bone regeneration in post-

extraction sockets[129]. The formulation was designed to be administrated in the target site wrapped in the L-PRF membrane, enhancing its well-known regenerative properties with the synergic action given by the simultaneous prolonged delivery of antibiotic and antioxidant compounds.

The ability of the minitablet to promote CUR and MTR permeation rather than penetration in the L-PRF clot was evaluated in agreement with FDA and CE approved protocol (Intra-spin®, Intra-lock, Salerno, Italy). An increased permeation of the antibiotic was noticed, demonstrating its ability to cross the L-PRF membrane. In contrast, it was not possible to detect CUR in the same compartment, probably due to its poor solubility in the acceptor fluid and high affinity with the membrane where it remained entrapped. The extrapolated flux highlighted that L-PRF acted as the limiting factor for the free diffusion of MTR from the minitablet towards the post-extraction socket. Due to the modulation over time of the antibiotic release and the spreading in the neighbor gingival tissues, the aseptic conditions might have been maintained for a prolonged time in the areas involved in tissue regeneration. Moreover, the accumulation of the drugs in the membrane could validate that the new nanocomposite system acts as a drug reservoir able to release the actives in the surrounding tissues slowly.

These permeations and the accumulation findings were strictly in accordance with our aim of obtaining a formulation able to slowly release anti-inflammatory and antibiotics agents, providing them in the target site for few days.

To exclude any cytotoxic effects induced by the formulation, the in vitro viability assay on normal stromal cells HS5 was performed testing Sponge-C-MTR and comparing the results to empty sponge, prepared by the same process but without CUR and MTR.

The results allowed defining the cytoprotective role of CUR and MTR. Although CUR is well known for the anti-cancer activity, this compound shows a biphasic effect on the stem cell proliferation, depending on the treatment concentrations and the type of stem cells used. It has been reported that bone marrow mesenchymal stem cells showed an increase in proliferation at CUR concentration up to 10µM, whereas a cytotoxic effect for higher concentrations [130]. In our experiments, the tested concentrations of CUR, ranged to 0.61 and 3.66 µM, were below than the cytotoxic condition, thus suggesting a protective effect of CUR on cells and making Sponge-C-MTR potentially useful for *in vivo* administration.

In the light of described results, it could be concluded that this synergistic effect can be a potential strategy to overcome the antibiotic resistance mechanism that may occur with the MTR oral administration and improve the CUR delivery, supporting and enhancing the role of hemocomponents for the tissue regeneration in the dental and oral fields.

Regarding the innovative protocol of guided bone regeneration studied, the promising results support the action of L-PRF and its derivates in bone regeneration and ridge preservation, beyond that the oral surgery in general. However, further studies will be necessary to provide a greater number of evidence and confirm the potential of this pioneering procedure.

CHAPTER 5

References

1. Ott, S. M. Cortical or Trabecular Bone: What's the Difference? *Am. J. Nephrol.* **47**, 373–375 (2018).
2. Stagi, S., Cavalli, L,. Iurato, C., Seminara, S., Brandi, M.L., de Martino, M. Bone metabolism in children and adolescents : main characteristics of the determinants of peak bone mass. **10**, 172–179 (2013).
3. Ralston, S. H. Bone structure and metabolism. *Medicine (Baltimore).* **41**, 581–585 (2013).
4. Tou, J. C. Resveratrol supplementation affects bone acquisition and osteoporosis: Pre-clinical evidence toward translational diet therapy. *Biochim. Biophys. Acta - Mol. Basis Dis.* **1852**, 1186–1194 (2014).
5. Dimitriou, R., Jones, E., Mcgonagle, D. & Giannoudis, P. V. Bone regeneration : current concepts and future directions. *BMC Med.* **9**, 66 (2011).
6. Diab, D. L. & Watts, N. B. Postmenopausal osteoporosis. 501–509 (2013).
7. Titorencu, I., Pruna, V. & Jinga, V. V. Osteoblast ontogeny and implications for bone pathology : an overview. 23–33 (2014).
8. Carl-Magnus Bäckesjö, Yan Li, Urban Lindgren. Activation of Sirt1 Decreases Adipocyte Formation During Osteoblast Differentiation of Mesenchymal Stem Cells. *J. BONE Miner. Res.* **Volume 21**, (2006).
9. Durbin, S. M., Jackson, J.R., Ryan, M.J., Gigliotti, J.C., Alway, S.E., Tou, J.C. Resveratrol supplementation preserves long bone mass, microstructure, and strength in hindlimb-suspended old male rats. *J. Bone Miner. Metab.* **32**, 38–47 (2014).
10. Baron, R., Rawadi, G. & Roman-Roman, S. B. T.-C. T. in D. B. Wnt Signaling: A Key Regulator of Bone Mass. in **76**, 103–127 (2006).
11. Bartell, S. M., Kim, H.N., Ambrogini, E., Han, L., Iyer, S., Serra Ucer, S., Rabinovitch, P., Jilka, R.L., Weinstein, R.S., Zhao, H., O'Brien, C.A., Manolagas, S.C., Almeida, M. FoxO proteins restrain osteoclastogenesis and bone resorption by attenuating H 2 O 2 accumulation. (2014).
12. Baron, R. & Rawadi, G. Minireview : Targeting the Wnt-Catenin Pathway to Regulate

Bone Formation in the Adult Skeleton. **148**, 2635–2643 (2007).

13. Chu, T. M. G., Liu, S. S. Y. & Babler, W. J. *Craniofacial Biology, Orthodontics, and Implants*. *Basic and Applied Bone Biology* (Elsevier Inc., 2013).
14. Jiang, N., Guo, W., Chen, M., Zheng, Y., Zhou, J., Kim, S.G., Embree, M.C., Songhee Song, K., Marao, H.F., Mao, J.J. Periodontal Ligament and Alveolar Bone in Health and Adaptation: Tooth Movement. *Front. Oral Biol.* **18**, 1–8 (2015).
15. Gonçalves, L. S., Gonçalves, B. M. L. & Fontes, T. V. Periodontal disease in HIV-infected adults in the HAART era: Clinical, immunological, and microbiological aspects. *Arch. Oral Biol.* **58**, 1385–1396 (2013).
16. Gulabivala, K. & Ng, Y. L. Tooth organogenesis, morphology and physiology. *Endod. Fourth Ed.* 2–32 (2014).
17. Ramalingam, S., Sundar, C., Jansen, J. A. & Alghamdi, H. Alveolar bone science: Structural characteristics and pathological changes. *Dental Implants and Bone Grafts: Materials and Biological Issues* (Elsevier Ltd., 2019).
18. Hughes, F. J. Periodontium and Periodontal Disease. *Stem Cell Biology and Tissue Engineering in Dental Sciences* (Elsevier Inc., 2015).
19. Sodek, J. & McKee, M. D. Molecular and cellular biology of alveolar bone. *Periodontol. 2000* **24**, 99–126 (2000).
20. Martinez, L. M. Mesenchymal Stem Cells as Regulators of the Bone Marrow and Bone Components. *Mesenchymal Stromal Cells as Tumor Stromal Modulators* (Elsevier, 2016).
21. Boyce, B. F., Yao, Z. & Xing, L. Osteoclasts have multiple roles in bone in addition to bone resorption. *Crit. Rev. Eukaryot. Gene Expr.* **19**, 171–180 (2009).
22. Matalová, E., Lungová, V. & Sharpe, P. Development of Tooth and Associated Structures. *Stem Cell Biol. Tissue Eng. Dent. Sci.* 335–346 (2015).
23. Könönen, E., Gursoy, M. & Gursoy, U. Periodontitis: A Multifaceted Disease of Tooth-Supporting Tissues. *J. Clin. Med.* **8**, 1135 (2019).
24. Jaws, E., Pietrokovski, J., Starinsky, R. & Arensburg, B. Morphologic Characteristics of Bony. **16**, 141–147 (2007).
25. Aydin, U., Bulut, A. & Bulut, O. E. Assessment of maxillary and mandibular bone quality Learning objectives. *Eur. J. Radiol.* (2017).
26. Isik, B. K., Gürses, G. & Menziletoglu, D. Acutely infected teeth: to extract or not to

extract? *Braz. Oral Res.* **32**, e124 (2018).

27. Alzahrani, A. A., Murriky, A. & Shafik, S. Influence of platelet rich fibrin on post-extraction socket healing: A clinical and radiographic study. *Saudi Dent. J.* **29**, 149–155 (2017).
28. Popelut, A., Rousval, B., Fromentin, O., Feghali, M., Mora, F., Bouchard, P. Tooth extraction decision model in periodontitis patients. *Clin. Oral Implants Res.* **21**, 80–89 (2010).
29. Sadry, S. Orthodontic Approach in Facial and Dental Trauma. *Trauma Dent.* (2019). doi:10.5772/intechopen.83015
30. Tabrizi, R., Karagah, T., Shahidi, S. & Zare, N. Does platelet-rich plasma enhance healing in the idiopathic bone cavity? A single-blind randomized clinical trial. *Int. J. Oral Maxillofac. Surg.* **44**, 1175–1180 (2015).
31. Taberner-Vallverdú, M., Sánchez-Garcés, M. Á. & Gay-Escoda, C. Efficacy of different methods used for dry socket prevention and risk factor analysis: A systematic review. *Med. Oral Patol. Oral Cir. Bucal* **22**, e750–e758 (2017).
32. Roberts, G., Scully, C., Shotts, R. Dental emergencies. *The ABC of Oral Health.* **67**, 49 (2002).
33. Pagni, G., Pellegrini, G., Giannobile, W. V. & Rasperini, G. Postextraction alveolar ridge preservation: Biological basis and treatments. *Int. J. Dent.* **2012**, (2012).
34. Bodic, F., Hamel, L., Lerouxel, E., Baslé, M. F. & Chappard, D. Bone loss and teeth. *Jt. Bone Spine* **72**, 215–221 (2005).
35. Trombelli, L., Farina, R., Marzola, A., Bozzi, L., Liljenberg, B., Lindhe, J. Modeling and remodeling of human extraction sockets. *J. Clin. Periodontol.* **35**, 630–639 (2008).
36. Van Der Weijden, F., Dell'Acqua, F. & Slot, D. E. Alveolar bone dimensional changes of post-extraction sockets in humans: A systematic review. *J. Clin. Periodontol.* **36**, 1048–1058 (2009).
37. Barone, A., Ricci, M., Calvo-Guirado, J. L. & Covani, U. Bone remodelling after regenerative procedures around implants placed in fresh extraction sockets: An experimental study in Beagle dogs. *Clin. Oral Implants Res.* **22**, 1131–1137 (2011).
38. Ozcan, G. & Sekerci, A. E. Classification of alveolar bone destruction patterns on maxillary molars by using cone-beam computed tomography. *Niger. J. Clin. Pract.* **20**, 1010–1019 (2017).

39. John, V., Weddell, J. A., Shin, D. E. & Jones, J. E. Chapter 14 - Gingivitis and Periodontal Disease. in (ed. Dean, J. A. B. T.-M. and A. D. for the C. and A. (Tenth E.) 243–273 (Mosby, 2016). doi:https://doi.org/10.1016/B978-0-323-28745-6.00014-4
40. Covani, U., Cornelini, R. & Barone, A. Bucco-Lingual Bone Remodeling Around Implants Placed into Immediate Extraction Sockets: A Case Series. *J. Periodontol.* **74**, 268–273 (2003).
41. Kyriakidou, E., O'Connor, N., Malden, N. & Lopes, V. Bone defects of the jaws: Moving from reconstruction to regeneration. *Dent. Update* **41**, 613–622 (2014).
42. Horowitz, R., Holtzclaw, D. & Rosen, P. S. A review on alveolar ridge preservation following tooth extraction. *J. Evid. Based. Dent. Pract.* **12**, 149–160 (2012).
43. Retzepi, M. & Donos, N. Guided Bone Regeneration: Biological principle and therapeutic applications. *Clin. Oral Implants Res.* **21**, 567–576 (2010).
44. Whetman, J. & Mealey, B. L. Effect of Healing Time on New Bone Formation After Tooth Extraction and Ridge Preservation With Demineralized Freeze-Dried Bone Allograft: A Randomized Controlled Clinical Trial. *J. Periodontol.* **87**, 1022–1029 (2016).
45. Liu, J. & Kerns, D. G. Mechanisms of Guided Bone Regeneration: A Review. *Open Dent. J.* **8**, 56–65 (2014).
46. Dahlin, C., Linde, A., Gottlow, J. & Nyman, S. Healing of bone defects by guided tissue regeneration. *Plastic and Reconstructive Surgery* **81**, 672–676 (1988).
47. Nyman, S., Karring, T., Lindhe, J. & Plantén, S. Healing following implantation of periodontitis-affected roots into gingival connective tissue. *Journal of Clinical Periodontology* **7**, 394–401 (1980).
48. Elgali, I., Omar, O., Dahlin, C. & Thomsen, P. Guided bone regeneration: materials and biological mechanisms revisited. *Eur. J. Oral Sci.* **125**, 315–337 (2017).
49. Wang, H. L. & Boyapati, L. 'pASS' principles for predictable bone regeneration. *Implant Dent.* **15**, 8–17 (2006).
50. Farzad, M. & Mohammad Mohammadi. Guided bone regeneration: A literature review. *JOHOE/Spring* **1**, 175–182 (2012).
51. Lekovic, V., Camargo, P.M., Klokkevold, P.R., Weinlaender, M., Kenney, E.B., Dimitrijevic, B., Nedic, M. Preservation of Alveolar Bone in Extraction Sockets Using Bioabsorbable Membranes. *J. Periodontol.* **69**, 1044–1049 (1998).

52. Soldatos, N. K., Stylianou, P., Koidou, V.P., Angelov, N., Yukna, R., Romanos, G.E. Limitations and options using resorbable versus nonresorbable membranes for successful guided bone regeneration. *Quintessence Int. (Hanover Park. IL)* **48**, 131–147 (2017).

53. Urban, I. A., Lozada, J. L., Jovanovic, S. A. & Nagy, K. Horizontal Guided Bone Regeneration in the Posterior Maxilla Using Recombinant Human Platelet-Derived Growth Factor: A Case Report. *Int. J. Periodontics Restor. Dent.* **33**, 421–425 (2013).

54. Dohan Ehrenfest, D. M., Rasmusson, L. & Albrektsson, T. Classification of platelet concentrates: from pure platelet-rich plasma (P-PRP) to leucocyte- and platelet-rich fibrin (L-PRF). *Trends Biotechnol.* **27**, 158–167 (2009).

55. Albanese, A., Licata, M. E., Polizzi, B. & Campisi, G. Platelet-rich plasma (PRP) in dental and oral surgery: From the wound healing to bone regeneration. *Immun. Ageing* **10**, 1 (2013).

56. Moraschini, V. & Barboza, E. S. P. Effect of autologous platelet concentrates for alveolar socket preservation: A systematic review. *Int. J. Oral Maxillofac. Surg.* **44**, 632–641 (2015).

57. Pal, U., Mohammad, S., Singh, R.K., Das, S., Singh, N., Singh, M. Platelet-rich growth factor in oral and maxillofacial surgery. *Natl. J. Maxillofac. Surg.* **3**, 118 (2012).

58. Del Fabbro, M., Corbella, S., Taschieri, S., Francetti, L. & Weinstein, R. Autologous platelet concentrate for post-extraction socket healing: a systematic review. *European journal of oral implantology* **7**, 333–344 (2014).

59. Andrade, C., Camino, J., Nally, M., Quirynen, M., Martínez, B., Pinto, N. Combining autologous particulate dentin, L-PRF, and fibrinogen to create a matrix for predictable ridge preservation: a pilot clinical study. *Clin. Oral Investig.* **24**, 1151–1160 (2020).

60. Sureshbabu, N. M., Selvarasu, K., Jayanth Kumar, V., Nandakumar, M. & Selvam, D. Concentrated growth factors as an ingenious biomaterial in regeneration of bony defects after periapical surgery: A report of two cases. *Case Rep. Dent.* **2019**, (2019).

61. Dohan, D. M., Choukroun, J., Diss, A., Dohan, SL., Dohan, AJ., Mouhyi, J., Gogly, B. Platelet-rich fibrin (PRF): A second-generation platelet concentrate. Part III: Leucocyte activation: A new feature for platelet concentrates? *Oral Surgery, Oral Med. Oral Pathol. Oral Radiol. Endodontology* **101**, (2006).

62. Choukroun, J., Adda, F., Schoeffler, C. & Vervelle, A. Une opportunit?? en paro-

implantologie: Le PRF. *Implantodontie* **42**, 55–62 (2001).

63. Dohan Ehrenfest, D. M., Del Corso, M., Diss, A., Mouhyi, J. & Charrier, J.-B. Three-Dimensional Architecture and Cell Composition of a Choukroun's Platelet-Rich Fibrin Clot and Membrane. *J. Periodontol.* **81**, 546–555 (2010).
64. Dohan Ehrenfest, D. M., de Peppo, G. M., Doglioli, P. & Sammartino, G. Slow release of growth factors and thrombospondin-1 in Choukroun's platelet-rich fibrin (PRF): A gold standard to achieve for all surgical platelet concentrates technologies. *Growth Factors* **27**, 63–69 (2009).
65. Castro, A., Cortellini, S., Temmerman, A., Li, X., Pinto, N., Teughels, W., Quirynen, M. Characterization of the Leukocyte- and Platelet-Rich Fibrin Block: Release of Growth Factors, Cellular Content, and Structure. *Int. J. Oral Maxillofac. Implants* **34**, 855–864 (2019).
66. Cortellini, S., Castro, A.B., Temmerman, A., Van Dessel, J., Pinto, N., Jacobs, R., Quirynen, M. Leucocyte- and platelet-rich fibrin block for bone augmentation procedure: A proof-of-concept study. *J. Clin. Periodontol.* **45**, 624–634 (2018).
67. de Almeida Barros Mourão, C. F., de Mello-Machado, R. C., Javid, K. & Moraschini, V. The use of leukocyte- and platelet-rich fibrin in the management of soft tissue healing and pain in post-extraction sockets: A randomized clinical trial. *J. Cranio-Maxillofacial Surg.* **48**, 452–457 (2020).
68. Schreml, S., Szeimies, R.M., Prantl, L., Karrer, S., Landthaler, M., Babilas, P. Oxygen in acute and chronic wound healing. *Br. J. Dermatol.* **163**, 257–268 (2010).
69. Schropp, L. Bone healing and soft tissue contour changes following single-tooth extraction: A clinical and radiographic 12-month prospective study. *J. Prosthet. Dent.* **91**, 92 (2004).
70. Sato, S., Fonseca, M. J. V., Ciampo, J. O. Del, Jabor, J. R. & Pedrazzi, V. Metronidazole-containing gel for the treatment of periodontitis: an in vivo evaluation. *Braz. Oral Res.* **22**, 145–150 (2008).
71. Haris, M. & Panickal, D. M. Role of Metronidazole as a Local Drug Delivery in the Treatment of Periodontitis:A Review. *Int. J. Oral Heal. Med. Res.* **3**, 141–145 (2017).
72. Rajagopalan, A. & Thomas, D. J. T. Effectiveness of Metronidazole as Local Drug Delivery in Periodontal Diseases – A Review. *IOSR J. Dent. Med. Sci.* **13**, 25–28 (2014).

73. Domazetovic, V., Marcucci, G., Iantomasi, T., Brandi, M. L. & Vincenzini, M. T. Oxidative stress in bone remodeling : role of antioxidants. *Clin. Cases Miner. Bone Metab.* 209–216 (2017).
74. Akbik, D., Ghadiri, M., Chrzanowski, W. & Rohanizadeh, R. Curcumin as a wound healing agent. *Life Sci.* **116**, 1–7 (2014).
75. Nagpal, M. & Sood, S. Role of curcumin in systemic and oral health: An overview. *J. Nat. Sci. Biol. Med.* **4**, 3–7 (2013).
76. Mitic, A., Todorovic, K., Stojiljkovic, N., Stojanovic, N., Ilic, S., Todorovic, A., Stojnev, S. Beneficial effects of curcumin on the wound-healing process after tooth extraction. *Nat. Prod. Commun.* **12**, 1905–1908 (2017).
77. Rohanizadeh, R., Deng, Y. & Verron, E. Therapeutic actions of curcumin in bone disorders. *Bonekey Rep.* **5**, 1–7 (2016).
78. Dave, D. H., Patel, P., Shah, M., Dadawala, S.M., Saraiya, K, Sant, A.V. Comparative Evaluation of Efficacy of Oral Curcumin Gel as an Adjunct to Scaling and Root Planing in the Treatment of Chronic Periodontitis. *Adv Hum. Biol.* 64–69 (2018).
79. Swain, S., Beg, S. & Babu, S. M. Liposheres as a Novel Carrier for Lipid Based Drug Delivery : Current and Future Directions. 59–71 (2016).
80. Hasan, A., Morshed, M., Memic, A., Hassan, S., Webster, T. J., & Marei, H. E. Nanoparticles in tissue engineering: Applications, challenges and prospects. *Int. J. Nanomedicine* **13**, 5637–5655 (2018).
81. Mu, A., Schwarz, C. & Mehnert, W. Solid lipid nanoparticles (SLN) for controlled drug delivery – Drug release and release mechanism. **45**, 149–155 (1998).
82. Müller, R. H., Radtke, M. & Wissing, S. a. [1] R.H. Müller, M. Radtke, S. a Wissing, Solid lipid nanoparticles (SLN) and nanostructured lipid carriers (NLC) in cosmetic and dermatological preparations., Adv. Drug Deliv. Rev. 54 Suppl 1 (2002) S131-55. http://www.ncbi.nlm.nih.gov/pubmed/12460720.So. *Adv. Drug Deliv. Rev.* **54 Suppl 1**, S131-55 (2002).
83. Patel, D. Development & Screening Approach for Lipid Nanoparticle: A Review. *Int J Innov. Pharm Sci* **2**, 27–32 (2013).
84. Hazzah, H. A., Farid, R. M., Nasra, M. M. A., El-massik, M. A. & Abdallah, O. Y. Lyophilized sponges loaded with curcumin solid lipid nanoparticles for buccal delivery : Development and characterization. **492**, 248–257 (2015).

85. Qian, Z., Dai, M., Zheng, X., Xu, X., Kong, X., Li, X., Guo, G., Luo, F., Zhao, X., Wei, Y.Q., Qian, Z. Chitosan-alginate sponge: Preparation and application in curcumin delivery for dermal wound healing in rat. *J. Biomed. Biotechnol.* **2009**, (2009).

86. Murgia, D., Angellotti, G., D'Agostino, F. & De Caro, V. Bioadhesive matrix tablets loaded with lipophilic nanoparticles as vehicles for drugs for periodontitis treatment: Development and characterization. *Polymers (Basel).* **11**, 1–20 (2019).

87. Murgia, D., Angellotti, G., Conigliaro, A., Carfi Pavia, F., D'Agostino, F., Contardi, M., Mauceri, R., Alessandro, R., Campisi, G., De Caro, V. Development of a multifunctional bioerodible nanocomposite containing metronidazole and curcumin to apply on l-PRF clot to promote tissue regeneration in dentistry. *Biomedicines* **8**, 1–27 (2020).

88. Almeida, H. Lobão, P., Frigerio, C., Fonseca, J., Silva, R., Sousa Lobo, J.M., Amaral, M.H. Preparation, characterization and biocompatibility studies of thermoresponsive eyedrops based on the combination of nanostructured lipid carriers (NLC) and the polymer Pluronic F-127 for controlled delivery of ibuprofen. *Pharm. Dev. Technol.* **22**, 336–349 (2017).

89. Shi, F., Shi, F., Zhao, J.H., Liu, Y., Wang, Z., Zhang, Y.T., Feng, N.P. Preparation and characterization of solid lipid nanoparticles loaded with frankincense and myrrh oil. *Int. J. Nanomedicine* **7**, 2033–2043 (2012).

90. Ho, M.H., Kuo, P.Y., Hsieh, H.J., Hsien, T.Y., Hou, L.T., Lai, J.Y., Wang, D.M., Kuo. P.Y., Hsieh, H.J., Hsien, T.Y., Hou, L.T., Lai, J.Y., Wang, D.M. Preparation of porous scaffolds by using freeze-extraction and freeze-gelation methods. *Biomaterials* **25**, 129–138 (2004).

91. Wang, Y.J., Pan, M.H., Cheng, A.L., Lin, L.I., Ho, Y.S., Hsieh, C.Y., Lin, J.K. Stability of curcumin in buffer solutions and characterization of its degradation products. *J. Pharm. Biomed. Anal.* **15**, 1867–1876 (1997).

92. Jakoi, A. M., Iorio, J. A. & Cahill, P. J. Autologous bone graft harvesting: a review of grafts and surgical techniques. *Musculoskelet. Surg.* **99**, 171–178 (2015).

93. Betz, R. R. Limitations of autograft and allograft: new synthetic solutions. *Orthopedics* **25**, s561-70 (2002).

94. Del Fabbro M., Gallesio G. & Mozzati M. Autologous platelet concentrates for bisphosphonate-related osteonecrosis of the jaw treatment and prevention . A

systematic review of the literature. *Eur. J. Cancer* **51**, 62–74 (2015).

95. Al-Hamed, F. S., Tawfik, M. A.-M., Abdelfadil, E. & Al-Saleh, M. A. Q. Efficacy of Platelet-Rich Fibrin After Mandibular Third Molar Extraction: A Systematic Review and Meta-Analysis. *J. oral Maxillofac. Surg. Off. J. Am. Assoc. Oral Maxillofac. Surg.* **75**, 1124–1135 (2017).
96. Canellas, J. V. D. S., Medeiros, P. J. D., Figueredo, C. M. D. S., Fischer, R. G. & Ritto, F. G. Platelet-rich fibrin in oral surgical procedures: a systematic review and meta-analysis. *Int. J. Oral Maxillofac. Surg.* **48**, 395–414 (2019).
97. Landry RG, Turnbull RS, H. T. Effectiveness of benzydamine HCL in the treatment of periodontal post-surgical patients. *Res Clin Forums* **10**, 105e118 (1998).
98. Fujioka-Kobayashi, M. *et al.* Optimized Platelet-Rich Fibrin With the Low-Speed *Periodontol.* **88**, 112–121 (2017).
99. Wang, X., Yang, Y., Zhang, Y. & Miron, R. J. Fluid platelet-rich fibrin stimulates greater dermal skin fibroblast cell migration, proliferation, and collagen synthesis when compared to platelet-rich plasma. *J. Cosmet. Dermatol.* **18**, 2004–2010 (2019).
100. Lourenço, E. S. Mourão, CF.AB, Leite, P.E.C., Granjeiro, J.M., Calasans-Maia, M.D., Alves, G.G. The in vitro release of cytokines and growth factors from fibrin membranes produced through horizontal centrifugation. *J. Biomed. Mater. Res. A* **106**, 1373–1380 (2018).
101. Ettl, T., Gosau, M., Sader, R. & Reichert, T. E. Jaw cysts - Filling or no filling after enucleation? A review. *J. Cranio-Maxillofacial Surg.* **40**, 485–493 (2012).
102. Ludovichetti, F. S., De Biagi, M., Bacci, C., Bressan, E. & Sivolella, S. Healing of human critical-size alveolar bone defects secondary to cyst enucleation: A randomized pilot study with 12 months follow-up. *Minerva Stomatol.* **67**, 148–155 (2018).
103. Cortellini, S., Castro, A.B., Temmerman, A., Van Dessel, J., Pinto, N., Jacobs, R., Quirynen, M. Leucocyte- and platelet-rich fibrin block for bone augmentation procedure: A proof-of-concept study. *J. Clin. Periodontol.* **45**, 624–634 (2018).
104. Almeida Barros Mourão, C. F. De, Valiense, H., Melo, E. R., Freitas Mourão, N. B. M. & Maia, M. D. C. Obtenção da fibrina rica em plaquetas injetável (I-PRF) e sua polimerização com enxerto ósseo: Nota técnica. *Rev. Col. Bras. Cir.* **42**, 421–423 (2015).
105. Jiang, D., Dziak, R., Lynch, S. E. & Stephan, E. B. Modification of an osteoconductive

anorganic bovine bone mineral matrix with growth factors. *J. Periodontol.* **70**, 834–839 (1999).

106. Stephan, E. B., Jiang, D., Lynch, S., Bush, P. & Dziak, R. Anorganic bovine bone supports osteoblastic cell attachment and proliferation. *J. Periodontol.* **70**, 364–369 (1999).
107. Chenchev, I. L., Ivanova, V. V., Neychev, D. Z. & Cholakova, R. B. Application of Platelet-Rich Fibrin and Injectable Platelet-Rich Fibrin in Combination of Bone Substitute Material for Alveolar Ridge Augmentation - a Case Report. *Folia Med. (Plovdiv).* **59**, 362–366 (2017).
108. Kurien, B. T., Singh, A., Matsumoto, H. & Scofield, R. H. Improving the Solubility and Pharmacological Efficacy of Curcumin by Heat Treatment. *Assay Drug Dev. Technol.* **5**, 567–576 (2007).
109. Kharat, M., Du, Z., Zhang, G. & McClements, D. J. Physical and Chemical Stability of Curcumin in Aqueous Solutions and Emulsions: Impact of pH, Temperature, and Molecular Environment. *J. Agric. Food Chem.* **65**, 1525–1532 (2017).
110. Naksuriya, O., van Steenbergen, M. J., Torano, J. S., Okonogi, S. & Hennink, W. E. A Kinetic Degradation Study of Curcumin in Its Free Form and Loaded in Polymeric Micelles. *AAPS J.* **18**, 777–787 (2016).
111. Severino, P., Pinho, S. C., Souto, E. B. & Santana, M. H. A. Polymorphism, crystallinity and hydrophilic-lipophilic balance of stearic acid and stearic acid-capric/caprylic triglyceride matrices for production of stable nanoparticles. *Colloids Surfaces B Biointerfaces* **86**, 125–130 (2011).
112. Togashi, N. hiraishi, A., Nishizaka, M., Matsuoka, K., Endo, K., Hamashima, H., & Inoue, Y. Antibacterial activity of long-chain fatty alcohols against Staphylococcus aureus. *Molecules* **12**, 139–148 (2007).
113. Shetty, A. V, Thirugnanam, S., Dakshinamoorthy, G., Kajdacsy-balla, A. & Gnanasekar, M. 18 α -glycyrrhetinic acid targets prostate cancer cells by down-regulating inflammation-related genes. 635–640 (2011). doi:10.3892/ijo.2011.1061
114. Long, D. R., Mead, J., Hendricks, J. M., Hardy, M. E. & Voyich, J. M. aureus Survival and Attenuates Virulence Gene Expression. **57**, 241–247 (2013).
115. Damle, M. Glycyrrhiza glabra (Liquorice) - a potent medicinal herb. *Int. J. Herb. Med.* **2**, 132–136 (2014).

116. Haghshenas, V. Fakhari S, Mirzaie S, Rahmani M, Farhadifar F, Pirzadeh S, Jalili A. Glycyrrhetinic Acid Inhibits Cell Growth and Induces Apoptosis in Ovarian Cancer A2780 Cells. **4**, 437–441 (2014).
117. Tanideh, N., Rokhsari, P., Mehrabani, D. & Mohammadi, S. The Healing Effect of Licorice on Pseudomonas aeruginosa Infected Burn Wounds in Experimental Rat Model. 99–106 (2014).
118. Bhupinder, K. & Newton, M. J. Impact of Pluronic F-68 vs Tween 80 on Fabrication and Evaluation of Acyclovir SLNs for Skin Delivery. *Recent Pat. Drug Deliv. Formul.* **10**, 207–221 (2016).
119. de Oliveira, H. P., Tavares, G. F., Nogueiras, C. & Rieumont, J. Physico-chemical analysis of metronidazole encapsulation processes in Eudragit copolymers and their blending with amphiphilic block copolymers. *Int. J. Pharm.* **380**, 55–61 (2009).
120. Dallmann, A., Solodenko, J., Ince, I. & Eissing, T. Applied Concepts in PBPK Modeling: How to Extend an Open Systems Pharmacology Model to the Special Population of Pregnant Women. *CPT pharmacometrics Syst. Pharmacol.* **7**, 419–431 (2018).
121. Casale, M. Moffa A, Vella P, Sabatino L, Capuano F, Salvinelli B, Lopez MA, Carinci F, Salvinelli F. Hyaluronic acid: Perspectives in dentistry. A systematic review. *Int. J. Immunopathol. Pharmacol.* **29**, 572–582 (2016).
122. Contardi, M., Heredia-Guerrero JA, Perotto G, Valentini P, Pompa PP, Spanò R, Goldoni L, Bertorelli R, Athanassiou A, Bayer IS.Transparent ciprofloxacin-povidone antibiotic films and nanofiber mats as potential skin and wound care dressings. *Eur. J. Pharm. Sci. Off. J. Eur. Fed. Pharm. Sci.* **104**, 133–144 (2017).
123. De Caro, V., Murgia D, Seidita F, Bologna E, Alotta G, Zingales M, Campisi G. Enhanced In Situ Availability of Aphanizomenon Flos-Aquae Constituents Entrapped in Buccal Films for the Treatment of Oxidative Stress-Related Oral Diseases: Biomechanical Characterization and In Vitro/Ex Vivo Evaluation. *Pharmaceutics* **11**, 35 (2019).
124. Olsson, C., Jansson, H. & Swenson, J. The Role of Trehalose for the Stabilization of Proteins. *J. Phys. Chem. B* **120**, 4723–4731 (2016).
125. Sanad, R. A.-B. & Abdel-Bar, H. M. Chitosan-hyaluronic acid composite sponge scaffold enriched with Andrographolide-loaded lipid nanoparticles for enhanced

wound healing. *Carbohydr. Polym.* **173**, 441–450 (2017).

126. Wang, C., Luo W, Li P, Li S, Yang Z, Hu Z, Liu Y, Ao N. Preparation and evaluation of chitosan/alginate porous microspheres/Bletilla striata polysaccharide composite hemostatic sponges. *Carbohydr. Polym.* **174**, 432–442 (2017).
127. Loh, Q. L. & Choong, C. Three-dimensional scaffolds for tissue engineering applications: role of porosity and pore size. *Tissue Eng. Part B. Rev.* **19**, 485–502 (2013).
128. Kramschuster, A., Turng, L.-S. Fabrication of Tissue Engineering Scaffolds. *In Handbook of Biopolymers and Biodegradable Plastics;* (Ebnesajjad, S., Ed.;, 2013).
129. Cano-Durán, J. A., Peña-Cardelles, J. F., Ortega-Concepción, D., Paredes-Rodríguez, V. M., García-Riart, M., & López-Quiles, J. The role of Leucocyte-rich and platelet-rich fibrin (L-PRF) in the treatment of the medication-related osteonecrosis of the jaws (MRONJ). *J. Clin. Exp. Dent.* **9**, e1051–e1059 (2017).
130. Attari, F., Zahmatkesh, M., Aligholi, H., Mehr, S.E., Sharifzadeh, M., Gorji, A., Mokhtari, T., Khaksarian, M., Hassanzadeh, G. Curcumin as a double-edged sword for stem cells: Dose, time and cell type-specific responses to curcumin. *DARU, J. Pharm. Sci.* **23**, 2703–2706 (2015).

SCIENTIFIC PRODUCTS

Publications discussed in this thesis:

"Advance on Resveratrol Application in Bone Regeneration: Progress and Perspectives for Use in Oral and Maxillofacial Surgery."
D. Murgia, R. Mauceri, G. Campisi, V. De Caro. Biomolecules, 9, 94.

"Development of a Multifunctional Bioerodible Nanocomposite Containing Metronidazole and Curcumin to Apply on L-PRF Clot to Promote Tissue Regeneration in Dentistry."
D. Murgia, G. Angellotti, A. Conigliaro, F. Carfi Pavia, F. D'Agostino, M. Contardi, R. Mauceri, R. Alessandro, G. Campisi, V. De Caro. Biomedicines, 8, 425.

"Hydrophilic Sponges loaded with Curcumin solid lipid nanoparticles and Metronidazole applied on L-PRF clot to promote tissue regeneration in dentistry."
D. Murgia, R. Mauceri, C. Scialabba, G. Campisi, V. De Caro. Proceeding CRS Italy Chapter Annual Workshop 2018. Padova, 18-20 Ottobre 2018, published in Pharmaceutics.

"**Application of L-PRF for socket preservation of an anterior fractured tooth in a young patient: a case report."**
V. Crivello, D. Murgia, G. Oteri, L. Lo Russo, A. Cocco, P. Tozzo, G. Campisi, R. Mauceri. Abstract and Poster for the 27° National Congress of Oral Science University Professors.

"Leucocyte- and platelet-rich fibrin block: its use for the treatment of a large cyst with implant-based rehabilitation."
R. Mauceri, D. Murgia, O. Cicero, L. Paternò, L. Fiorillo, V. De Caro, G. Campisi. Medicina, 57, 180.

Publications not included in this thesis:

2019:

"Enhanced in situ availability of Aphanizomenon flos-aquae constituents entrapped in buccal films for the treatment of oxidative stress-related oral diseases. Biomechanical Characterization and In Vitro/Ex Vivo Evaluation."

V. De Caro, D. Murgia, F. Seidita, E. Bologna, G. Alotta, M. Zingales, G. Campisi. Pharmaceutics, 11(1):35.

"Bioadhesive Matrix Tablets Loaded with Lipophilic Nanoparticles as Vehicles for Drugs for Periodontitis Treatment: Development and Characterization."

D. Murgia, G. Angellotti, F. D'Agostino, V. De Caro. Polymers (Basel), 11(11):1801.

2020:

"Antibacterial PEGylated Solid Lipid Microparticles for Cosmeceutical Purpose: Formulation, Characterization, and Efficacy Evaluation."

G. Angellotti, D. Murgia, A. Presentato, M.C. D'Oca, A.G. Scarpaci, R. Alduina, M.V. Raimondi, V. De Caro. Materials (Basel), 13(9), E2073.

"Quercetin-based nanocomposites as a tool to improve dental disease management."

G. Angellotti, D. Murgia, G. Campisi, V. De Caro. Biomedicines, 8(11), 1–15, 504.

2021:

"The effect of microstructural differences of fibrin and self-assembling peptide hydrogels on dental pulp stem cells' behavior."

M. EzEldeen, B. Toprakhisar, D. Murgia, N. Smisdom, O. Deschaume, C. Bartic, H.V. Oosterwyck, R.V.S. Pereira, G. Opdenakker, I. Lambrichts, A. Bronckaers, R. Jacobs, J. Patterson. Scientific Report.

"3D-printing assisted fabrication of chitosan scaffolds from different sources and cross-linkers for dental tissue engineering."

M. EzEldeen, J. Loos, Z. M. Nejad, M. Cristaldi, D. Murgia, A. Braem, R. Jacobs. eCM Journal.